CoA REPORT AERO 211

THE COLLEGE OF AERONAUTICS
CRANFIELD

MEASUREMENT OF THE SYMMETRIC RESPONSE OF THE M.S. 760 'PARIS' AIRCRAFT TO ATMOSPHERIC TURBULENCE

by

D. A. Williams

CoA Report Aero 211

THE COLLEGE OF AERONAUTICS
CRANFIELD

MEASUREMENT OF THE SYMMETRIC RESPONSE OF THE M.S. 760 'PARIS' AIRCRAFT TO ATMOSPHERIC TURBULENCE

by

D. A. Williams

SUMMARY

Flight measurements have been made using the College of Aeronautics' M.S. 760 PARIS aircraft to determine the vertical component of atmospheric turbulence and the response of several aircraft parameters to that turbulence.

The measurements have been analysed to obtain power spectra, transfer functions, and coherence functions of the parameters relative to the centre of gravity acceleration. The results, together with resonance test results and estimated mass distributions, are intended to contribute to the experimental background necessary for verifying theoretical techniques for estimating the response of aircraft excited by atmospheric turbulence.

A report prepared under Ministry of Technology
Contract Number PD/28/034/ES

CONTENTS

1. INTRODUCTION

A design requirement for an aircraft is that it must be shown to be capable of withstanding the loads induced by atmospheric turbulence. Both the Federal Aviation Agency in the United States and the Air Registration Board in Great Britain require this demonstration to be implemented by calculating the response of the aircraft to a single gust of specified shape and amplitude and showing that the loads induced by the gust are not sufficient to cause structural failure.

A single gust is rarely, if ever, encountered in practice and the Federal Aviation Agency has proposed a supplementary requirement whereby the structural integrity of an aircraft should be further demonstrated by calculations based upon statistical descriptions of atmospheric turbulence. Such calculations would require accurate estimates of the response of the aircraft in the form of transfer functions. Examples of calculations to demonstrate the structural integrity of an aircraft using the statistical concept of atmospheric turbulence are contained in References 6 and 7.

The response of an aircraft to a single gust is conventionally computed by numerical integration of the equations of motion in the time domain. Because of the uncertainty associated with estimates of aerodynamic forces in the time domain, it has been suggested in Reference 8 that the response to a single gust may be computed more accurately by transforming the appropriate transfer function into the time domain.

The computation of transfer functions required for both of the above mentioned processes is complex and has become practicable only with the advent of large and fast digital computers. If confidence is to be placed in such computations it is essential that they be checked by comparing transfer functions obtained by them for existing aircraft whose characteristics are known with experimental results obtained from flights in appropriate conditions.

To date very few experimentally obtained descriptions of the response of an aircraft in atmospheric turbulence have been published, only one of which, Reference 9, includes descriptions of associated turbulence velocity characteristics and estimates of the coherence functions necessary for determining the significance of the results. Measurements of the symmetric component of excitation and response of an M.S. 760 PARIS aircraft whilst flying in atmospheric turbulence are described in this report together with the results, in the form of power spectra and transfer functions, of analyses performed on selected samples of the measurements. The technique used for the analysis is described, as is an estimation of the accuracy of the results. Mode shapes and associated inertias and frequencies for the range of interest are included, together with stability and control data, providing sufficient information to allow the comparison of results obtained from a theoretical analysis with those presented herein.

The work described in this report was sponsored by the Ministry of Technology under Contract Number PD/28/034.

2. AIRCRAFT GROUND RESONANCE TESTS

In order to determine the structural characteristics of the M.S. 760 PARIS, the aircraft was ground resonance tested in two typical flight configurations to obtain the symmetric resonance mode shapes and frequencies occuring between 3 Hz and 30 Hz. A description of the resonance test procedure appears as Appendix A.

Many modes were excited in the initial frequency sweep. Some of these were local modes and could clearly be neglected, but others were asymmetric modes in which, for example, antisymmetric tailplane bending was strongly excited by symmetric wing excitation, indicating that the aircraft was asymmetric. All modes excited, with the quite marked exceptions of the ones listed in Table 3, exhibited large phase differences between the response of two points at extremities of the aircraft and so were readily identifiable.

Resonant frequencies, assumed to be natural frequencies, and damping ratios obtained from transfer functions are shown in Table 2, whilst the measured mode shapes are listed in Tables 9 and 10. The mode shapes were used with the weight distribution given in Tables 11 and 13 to determine generalised inertia matrices for the two configurations considered. These matrices are shown in Tables 7 and 8.

3. INSTRUMENTATION

Details of the quantities recorded in flight, together with ground calibrations, were described in Reference 1. For completeness, these details are summarised below.

Eleven channels of flight data were recorded, in frequency modulated form, on to magnetic tape using a Flexonics A4011 fourteen channel split stack tape recorder. Also recorded were a voice channel for identification purposes and a 12KHz crystal controlled reference signal. Recorder channel allocation and scale factors are shown in Table 1.

The flight tape recorder was a "record only" device, and flight recordings were replayed using a Flexonics M400 machine. The pitch of the two head stacks on this machine differed from that of the flight recorder and so, in order to preserve time correlation between channels on the two stacks, the centre of gravity acceleration signal was chosen as a reference and recorded on two channels, one on each head stack.

The record/replay system was calibrated by switching the tape recorder modulation inputs to a common rail and then switching controlled reference voltages to the rail whilst recording. The reference levels were nominally zero volts, plus one volt and minus one volt, and covered about two thirds of the linear range of the modulators. Switching for the calibration was controlled by a single four position switch located on the tape recorder control box, thus allowing in-flight calibration of the system.

An unresolved difficulty encountered with the instrumentation was the breakthrough of R/T transmission from the aircraft causing apparent overloads on certain channels. This fault was countered by an arrangement between the pilot and the ground controller, whereby no airborne transmissions, such as acknowledgements of positional information, should expected during the execution of a task.

Upon analysis of Flights 5 and 6 it was discovered that significant antisymmetric components were present in channel 8, the recording of tail-plane bending moment. It was deducted that a strain gauge had become inoperative, and all the strain gauges associated with the measurement of bending moment channel were replaced. Recalibration of the bending moment channel revealed that the strain gauges being mounted on the tail-plane pivot trunnion were, in fact, measuring tail-plane rear spar load. It was decided not to alter the strain gauge locations as the chordwise position of the centre of tail-plane pressure was considered to be as interesting as its spanwise position.

4. FLIGHT TEST TECHNIQUES

All flights took place with a pilot and an observer. They were flown out of Cranfield and under the surveillance of the Cranfield Radar Unit. The tape recorder was normally switched on for the whole of each flight, during which the pilot noted orally flight conditions, and control and trim surface movements, whilst the observer noted forward airspeed, altitude, fuel used and flight duration at thirty second intervals.

Several tasks were set to the pilot during the period of flight testing. They were:-

4.1 To record onto all data channels known voltage levels in order to calibrate the record/replay system. This task was the first performed on each flight, and for the period of the task, about three minutes, the pilot was instructed not to perform violent manoeuvres.

4.2 The pilot was instructed to trim the aircraft to fly straight and level hands off at a chosen forward airspeed and altitude in calm air conditions, and then perform both single and multiple cycles of sinusoidal pitching manoeuvres about the steady condition, termed "rollercoasters", with periods ranging from two seconds to ten seconds. The purpose of this task was to allow the technique used for the reconstitution of gust velocity to be checked.

Accomplishment of this task without overloading the instrumentation proved difficult, and after several unsuccessful in-flight attempts a simple manoeuvre director was developed. The director comprised a variable frequency oscillator and the pilot was required to match the output of the oscillator with a measured response of the aircraft. Several forms of presentation were evaluated with the aid of a flight simulator, the one finally selected requiring the pilot to null the reading of a meter displaying the difference between demand and measured centre of gravity acceleration. Once the gain and sensitivity of the device had been optimised no difficulty was experienced in accomplishing the task.

4.3 The pilot was instructed to trim the aircraft to fly straight and level hands off at a chosen forward airspeed and altitude in turbulent conditions, and then to maintain a constant heading, airspeed and altitude for a period of five minutes whilst controlling the aircraft in the normal manner.

Atmospheric conditions giving rise to large areas of turbulence of sufficient intensity occured very infrequently and, normally, at very short notice. It was discovered, however, that adequate conditions could be expected at low altitude in the shear layer associated with high wind conditions, and flights were made to accomplish task 4.3 whenever the mean surface wind rose to over thirty knots.

4.4 The pilot was instructed to trim the aircraft to fly straight and level hands off at a chosen forward airspeed and altitude in turbulent conditions and allow it to fly for as long as possible without touching the controls.

This task proved very difficult to accomplish because large amplitude phugoid oscillations were quickly excited by the turbulence causing large changes both in altitude and forward airspeed.

A list of flights performed together with the relevant details concerning them is included as Appendix B.

5. THE ANALYSIS OF FLIGHT RECORDS

The object of the analysis was to reconstitute the vertical component of turbulence velocity from the flight records, and to describe the resulting time history and the response of the various measured quantities to that time history.

The random nature of the turbulence precluded an exact description of either the turbulence velocity or the measured aircraft responses but, by assuming the turbulence to be continuous and stationary and the aircraft responses could be described by their respective power spectral densities. Furthermore, the characteristics of the aircraft responses to turbulence could be described in the form of transfer functions deduced by determining their cross spectral densities with respect to the turbulence.

In the present exercise the vertical component of gust velocity was not recorded directly so, for the reasons given in Section 3, centre of gravity acceleration was chosen as a reference, and the transfer functions of other quantities computed relative to it. The transfer function of the centre of gravity acceleration relative to the vertical component of turbulence velocity was then computed to allow the transfer function of any quantity to be calculated relative to the vertical component of gust velocity, provided that the two appropriate coherence functions were sufficiently high.

The vertical component of gust velocity was obtained by using the recordings of boom acceleration and centre of gravity pitch rate to remove the effects of the motion of the aircraft from the recording of vane incidence. The details of this reconstitution are shown in Appendix C. It was considered to be vitally important to match the scalings of the three channels involved as accurately as possible, and for this reason the "roller-coaster" manoeuvres performed in flight were used to check that aircraft motion in calm air conditions gave zero reconstituted gust velocity at least over a frequency range 0.1 Hz to 0.5 Hz.

Equipment necessary for the computation of power and cross spectra was not at first available on site and the initial evaluation of power spectral estimates was performed by O.N.E.R.A. in France. Meanwhile the expected arrival of a suitable on site analysis facility failed to materialise, and several alternatives were investigated. The technique finally adopted, described in Appendix C, was implemented using a general purpose analogue computer and direct inteegration to determine the average required. The analysis using this technique proved to be very lengthy on its basic form, but was rendered practical by re-recording the chosen sample onto a magnetic tape loop, and replaying the tape loop for analysis purposes at four times the recorded speed. The procedure used for the spectral analysis of the selected samples is detailed in Appendix D.

The selection of samples was made initially by visual examination of a pen recorder trace of the centre of gravity acceleration time history for the whole of the particular flight. Likely samples were than examined in more detail for stationarity and the best examples chosen for detailed analysis. Two examples from Flight 6 and two from Flight 9 were chosen for analysis, one sample from each flight being taken from a part of the flight when the pilot was controlling the aircraft and the other sample in each case being taken from a part of the flight when the aircraft was in the "stick free" condition. By coincidence both "hands on" samples were of three minutes duration and both "hands off" samples were of ninety seconds duration. Thus, allowing thirty seconds for the delay of analyser filter transients, averaging times achieved were one hundred and fifty seconds for the "hands on" sample and sixty seconds for the "hands off" sample.

Raw estimates obtained by the procedure detailed in Appendix D included the effects of individual transducer transfer functions and, in some cases, the effects of high pass filters used to protect the analyser from possible overload. The raw estimates were processed to remove these effects before plotting. Processed power spectral densities are shown in Figures 7 to 21, and processed transfer functions and coherence functions are shown in Figures 22 to 68. In these figures the moduli of the transfer functions are denoted coherent amplitude spectra to distinguish them from amplitude spectra obtained by square rooting the ratios of the two power spectra. Transducer transfer functions were obtained from Reference 1 with the exception of that for the centre of gravity accelerometer which was obtained from a re-calibration, the results of which are shown in Figure 69.

Effective in-flight damping coefficients associated with modes excited by the vertical component of atmospheric turbulence were computed from power spectral estimates using the technique described in Appendix C. Estimated effective damping coefficients, together with associated natural frequencies, are compared with ground resonance test results in Table 3.

Estimates of the root mean square values of the vertical component of turbulence velocity were obtained by the substitution of the spectral density value of the appropriate turbulence velocity at 1.0 Hz into Equation C.40. Assuming the forward airspeed of the aircraft to be 515 feet per second T.A.S. and the characteristic gust length to be 6.44 feet per second for Flight 6, and 6.66 feet per second for Flight 9.

6. ACCURACY OF RESULTS

The overall accuracy of the results was extremely difficult to express in a convenient form. Errors were, in fact, divided into three categories, scale errors, variance errors, and bias errors. Scale errors arose only from inaccuracies in calibrations and scaling, and were independent of frequency. Estimates for the values of the various components are included in Table 6, and gave values for overall scale errors for power spectral density estimates of 8% for tailplane total load, 12% for tailplane rear spar shear, and 6% for other channels. The corresponding maximum errors of scale for transfer function estimates were 7%, 9% and 6% respectively.

Variance errors arose both from the analysis technique employed and from the implementation of that technique. Those due to the technique varied with frequency, as shown in Table 5, whilst those due to the implementation were independent of frequency. Estimates for values of the variance error due to implementation are included in Table 6, and give overall values for this component of 7% for power spectral density estimates and approximately 7 divided by the local value of coherence function for transfer function estimates.

The most difficult type of error to evaluate was bias error. Expressions for estimating the maximum bias error occuring in power spectral density estimates were developed in Appendix D after making somewhat sweeping assumptions. Fortunately bias errors should only be significant at frequencies close to resonance. Estimated maximum values for the significant modes are shown in Table 5.

One further source of error was extraneous noise present in the data. This arose particularly from the re-recording technique adopted for the analysis and could give large values of error at very low levels of power spectral density.

7. DISCUSSION

Examination of reconstituted gust velocity time histories computed from roller-coaster manoeuvres indicated that, at least for frequencies between 0.1 Hz and 0.5 Hz, the technique used for the reconstitution of the vertical component of gust velocity and the relevant calibrations presented in Reference 1 were of satisfactory accuracy. It was suspected, however, that the accuracy of the reconstitution as implemented in the present case deteriorated at higher frequencies where local boom and fuselage rotations about the transverse axis could not be neglected. It was considered that the accuracy of the reconstitution of these frequencies could be improved by installing a pitch rate gyro in the boom close to the vane position and using the output of this device, rather than that of the centre of gravity pitch rate gyro, to compute the relative boom incidence time history.

The estimation of power and cross spectral density proved to be a lengthy process using the method adopted for the present analysis. The use of a general purpose analogue computer for the implementation allowed, however, a high degree of control over the voltage levels in the analyser and thus an accuracy, so far as the analyser was concerned, which was substantially independent of the level of power spectral density. The results obtained using the techniques described in Appendix D were in excellent agreement with those obtained by O. N. E. R. A. during the initial analysis.

Errors present in computer estimates of power spectra and transfer functions comprised scale errors, variance errors, and bias errors. Of these, bias errors posed the greatest problem as they were proportional to the normalised rate of change of slope with frequency, according to Reference 2, and this made the estimation of effective damping coefficients a difficult task. Assuming a simplified spectral shape typical of those expected from accelerometer outputs at frequencies close to a resonance, expressions for a maximum bias error were obtained using both the method described in Reference 2, and a more accurate method developed in Appendix D. The former method was strictly applicable only when the bias error was very small, whilst the second method was designed to be applicable for all values of bias error, provided only that the bandwidth of the filter was small. It was noted with interest that the two expressions did not converge as the bias error tended to zero, a fact which was thought to be due to the assumption made for the derivation of the method of Reference 2. An incidental point arising from an examination of the derivation of the method of Reference 2 was that no justification could be found for using the equivalent statistical bandwidth for the final expression for bias error.

Corrections for bias error in estimates of the effective damping ratio of aircraft modes obtained from transfer functions proved to be very difficult to evaluate with the type of filter employed in the present exercise. Consequently effective damping ratios were obtained from power spectral estimates, and corrected using an expression developed in Appendix C.

A difficulty entountered in the analysis arose from the technique of re-recording the chosen sample before analysis. The process of re-recording introduced variations of signal level causing occasional "drop-out" of the descriminator output. The discriminators used were of a type which produced a large output voltage when no input was being sensed, and consequently drop-outs appeared at the input to the analyser as large amplitude pulses. When the gain of the analyser was high, the ringing of the filters caused by these pulses could produce an apparent increase in the value of a power spectral density estimate. Examination of the re-recordings indicated that there was no correlation between drop-outs occuring on different tracks, implying that they would not affect cross spectral density estimates. Thus the effect of drop-outs was to increase the value of a power spectral estimate particularly when this was small and to decrease the corresponding value of coherence and, when the power spectral density of the reference channel was effected, transfer function.

It became apparent during the analysis that the choice of the centre of gravity accelerometer as the reference channel was somewhat unfortunate. Firstly the accelerometer had a very low cut-off frequency, as may be seen from Figure 69, necessitating large corrections to transfer functions, and secondly the low coherence values at high frequencies rendered the computation of the transfer function of a quantity relative to the turbulence from transfer functions of the quantity relative to the centre of gravity acceleration and the centre of gravity acceleration relative to the turbulence to be of doubtful accuracy at these frequencies.

8. CONCLUSIONS AND RECOMMENDATIONS

Power spectra and transfer functions have been determined for the symmetric component of the response of an M.S. 760 PARIS aircraft from records obtained during flights in atmospheric turbulence. Coherence functions deduced from the results indicated that the results are of good accuracy, at least up to 10 Hz. With the information from the resonance tests described in Appendix A and the stability and control data presented in Appendix C, the results provide the necessary information to check the validity of theoretical techniques for the estimation of the symmetric component of the response of an aircraft excited by atmospheric turbulence.

The choice of the centre of gravity accelerometer as a reference channel proved somewhat troublesome, and it is considered that in-flight reconstitution of gust velocity for use as the reference channel would be of benefit for future work.

The College of Aeronautics now possesses facilities for the analysis of random data and an instrumented aircraft which, with some modifications and additions, could be used to determine the response of an aircraft to the lateral component of atomospheric turbulence. In view of this and because of the present uncertainty concerning the strength of T-tailed aircraft in turbulent conditions, it is recommended that the present exercise be extended to cover the measurement and analysis of the response of the M.S. 760 PARIS aircraft to the lateral component of turbulence.

9. REFERENCES

1.	Clark, B.S.	M.S. 'PARIS' Response Atmospheric Turbulence (Interim Memo)	C.o.A.Memo No. 121
2.	Bendat, J.S. Piersol, A.G.	Measurement and Analysis of Random Data	Wiley, 1966
3.	Williams, D.A.	Techniques for the Analysis of Random Data Obtained from Flight Tests at Atmospheric Turbulence	Paper presented at the 5th International Aerospace Instrumentation Symposium
4.	Barber, D.L.A.	A high Speed Analogue Multiplier	Electronic Engineering April, 1963
5.	Howe, J.M.	A Select Bibliography on Power Spectral Analysis	Hertfordshire County Council Technical Information Service
6.	Hoblit, F.M. et al.	Development of a Power Spectral Gust Design Procedure for Civil Aircraft.	FAA-ADS-53 1966
7.	Fuller, J.R. et al.	Contribution to the Development of a Power Spectral Gust Design Procedure for Civil Aircraft	FAA-ADS-54 1966
8.	Mitchell, C.G.B.	Calculation of the Response of a Flexible Aircraft to Harmonic and Discrete Gusts by a Transform Method	R. & M. 3498
9.	Coleman, T.L. Press, H. Meadows, M.T.	An Evaluation of Effects of Flexibility on Wing Strains in Rough Air for a Large Swept-Wing Airplane by Means of Experimentally Determined Frequency Response Functions with an Assessment of Random-Process Techniques Employed.	NASA TR R-70 1960

10. ACKNOWLEDGEMENTS

The author would like to express his thanks to those who made possible the execution of the work described in this report. In particular he would like to thank

O.N.E.R.A., France, and especially Dr. G. Coupry and his colleagues for their generous hospitality and co-operation in performing the initial processing of results.

Hawker Siddeley Aviation Ltd., Hatfield, for allowing use of their English Electric KDF 9 digital computer.

Elliott Brothers, for the loan of analogue computers used in the development of the processing technique.

Mr. C.G.B. Mitchell, for his constant encouragement and many helpful suggestions.

11. NOMENCLATURE

C		A constant of integration introduced in Equation C1
G_1, G_2		Bandpass filter gains (equations D1 and D2)
$H\ (i\omega)$		Bandpass filter transfer function (equation C5)
K_1, K_2		Final outputs of spectral analyser integrators (equations D1 and D2)
L		Characteristic gust length (equation C41)
t		"real" time
T		Integration time
$T12(i\omega)$	=	${}_RT_{12}(\omega) + i_IT_{12}(\omega)$ System transfer function
$T_{(90)}(i\omega)$		Transfer function of 90^o phase shift filter (equation C22)
V		Time airspeed
w		Vertical component of gust velocity (equation C1)
X_1, X_2		Data calibrations (equations D1 and D2)
$y_1(t)$, $y_2(t)$		Data time histories
$y_{f_1}(t)$, $y_{f_2}(t)$		Bandpass filtered time histories
$\ddot{z}_v$		Vertical component of vane acceleration (equation C1)
β		Local incidence measured by vane (equation C1)
$\gamma(\omega)$		Coherence function (equation C12)
Δ		A factor defined in equation C34
$\epsilon(\omega)$		"Bias" error function, see Appendix E
ϵ_{var}		Variance errors (equation E15)
$\Delta\omega$, $\Delta\omega_1$, $\Delta\omega_2$		Small changes in frequency (equation C1)
$\dot{\theta}$		Centre of gravity pitch rate (equation C1)
$\phi_1(\omega)$		Excitation power spectral density (equation C3)
$\phi_2(\omega)$		Response power spectral density (equation C3)
τ		A time delay (equation C8)
ζ_1		Damping ratio of system mode (equation C24)
ζ		Damping ratio of filter (equation C33)
ω		Circular frequency
ω_1		Natural frequency of system mode (equation C24)
ω_o		Natural frequency of filter (equation C33)
Ω		Filter bandwidth (equation E6)
Ω_e		Equivalent filter bandwidth (equation E5)

APPENDIX A

DESCRIPTION OF GROUND RESONANCE TEST

A. 1 AIRCRAFT CONFIGURATIONS

The aircraft was tested in two fuel configurations, viz. with tip tanks empty, and with tip tanks full. For each configuration the aircraft was ballasted to simulate the pilot and observer, the instrumentation pack was installed, and a representative main fuel tank state was obtained by draining 300 litres from the fuel tank. The elevator was restrained from rotation during the resonance tests by a clamp positioned between the elevator horn and the tailplane.

A. 2 AIRCRAFT SUPPORTS

In an effort to minimise the effect of support constraints upon the mode measurements, the aircraft was mounted, with its undercarriage retracted, upon two large air bags, each extending from the centre line to approximately wing semispan and supporting the entire chord of the wing. The resulting nose down attitude was countered by the addition of a smaller air bag placed under the nose of the aircraft.

With the aircraft supported only by airbags it tended to wander slightly, endangering the exciters attached to it, so for the resonance test a small proportion of the weight of the aircraft was taken by an overhead safety sling.

A. 3 EXCITATION

Two Goodman electro-magnetic exciters were attached either to points on the wing near the outer edge of the aileron at about seventy per cent of local chord, or to the restraining brackets mounted between the elevator horn and the tailplane. The exciters were wired in parallel to the output of a Derritron 300 WT power amplifier which was driven by a Solartron OS103 decade oscillator. The exciters were assumed to have similar dynamic characteristics so that corrections to individual exciters were unnecessary.

A. 4 INDENTIFICATION AND MEASUREMENT OF MODES

A four phase output from the oscillator was used as a reference for a Solartron VP253 resolved components indicator. A measured signal input to this device could be output to an Y-X plotter in its real and imaginary component forms, thus providing a means for plotting directly the transfer function of the measured response relative to the oscillator input.

Aircraft modes were identified by attaching the exciters, and an accelerometer very close to one of them, firstly to the wing and then to the tailplane and, in each case, causing the oscillator to sweep slowly in frequency between 3Hz and 30Hz while the transfer function of the accelerometer output was being recorded. With the aid of the two transfer functions the primary aircraft modes could easily be identified and their natural frequencies and damping coefficients measured.

The measurement of a particular mode shape was made by exciting the aircraft at the better of the two excitation points for that mode, optimising the gain of the X-Y plotter, setting the oscillator frequency to the value previously determined for the resonant frequency of the mode, and by plotting, using the X-Y plotter, the vector response of the whole aircraft by attaching a roving accelerometer to each of a large number of marked measurement points and recording the transfer function of the point together with its appropriate identification number.

APPENDIX B

FLIGHTS ACCOMPLISHED

Flight Number 1. Date 16. 11. 66

Initial Fuel Condition	-	Full mains, empty tip tanks
Take off Weight	-	6877 lb.
Take off c. g. Position	-	114. 51 inches aft of datum
Tasks Performed	-	4. 1
		4. 2 at 250 kts. I. A. S. and 6, 000 ft.
		4. 3 at 250 kts. I. A. S. and 2, 500 ft.

Comments

Results from this flight were used for determining suitable instrumentation ranges. Only channels 1, 2, 3, 4, 6, 10, 12, and 14 were recorded.

Flight Number 2 Date 16. 11. 66

Initial Fuel Conditions	-	Full mains, empty tip tanks
Take off Weight	-	6877 lb.
Take off c. g. Position	-	114. 51 inches aft of datum
Tasks Performed		4. 1
		4. 2 at 250 kts. I. A. S. and 6, 000 ft.
		4. 3 at 250 kts. I. A. S. and 2, 500 ft.

Comments

This flight was a repeat of Flight 1 with the ranges of certain instruments changed. The roller coasters performed in the execution of Task 4. 2 were of 10 seconds period only, and the results were not satisfactory.

Flight Number 3 Date 16. 3. 67

Initial Fuel Conditions	-	Full mains, empty tip tanks
Take off Weight	-	6877 lb.
Take off c. g. Position	-	114. 51 inches aft of datum
Tasks Performed	-	4. 1
		4. 2 at 250 kts. I. A. S. and 6, 000 ft.
		4. 3 at 250 kts. I. A. S. and 2, 500 ft.
		4. 4 at 250 kts. I. S. A. and 2, 500 ft.

Comments

All instrumentation channels were recorded. Single roller coasters with periods ranging from 10 seconds to 2 seconds were performed for task 4. 2. Long period manoeuvres were found to be very uneven whilst short period manoeuvres overloaded certain channels. Turbulence levels measured in tasks 4.3 and 4.4 were very low, and trimming the aircraft to perform task 4.4 satisfactorily was found to be very difficult. Tape channels 7 and 8 were very noisy.

Flight Number 4 — Date 5. 4.67

Initial Fuel Conditions - Full mains, empty tip tanks
Take off Weight - 6877 lb.
Take off c.g. Position - 114.51 inches aft of datum

Tasks Performed - 4.1
4.2 at 250 kts. I.A.S. and 6,000 ft.

Comments

This flight was made in an attempt to accomplish task 4.2 successfully. The output from the pitch rate gyro was displayed on a meter so that the pilot could monitor his performance. The results showed some improvement over previous ones but were still not considered satisfactory. The noise present on tape channels 7 and 8 noted after Flight 3 had been cured by filtering the supplies to the demodulators.

Flight Number 5 — Date 12. 5.67

Initial Fuel Condition - Full mains, empty tip tanks
Take off Weight - 6877 lb.
Take off c.g. Position - 114.51 inches aft of datum

Tasks performed - 4.1
4.3 to 300 kts. I.A.S. and 2,500 ft.
4.4 at 300 kts. I.A.S. and 2,500 ft.

Comments

High levels of turbulence were found during this flight. All measurement channels were recorded successfully with the exception of channel 7 which was badly out of balance.

Flight Number 6 — Date 12.5.67

Initial Fuel Condition - Full mains, full tip tanks
Take off Weight - 7143 lbs.
Take off c.g. Position - 113.9 inches aft of datum

Tasks Performed - 4.1
4.3 at 300 kts. I.A.S. and 2,500 ft.
4.4 at 300 kts. I.A.S. and 2,500 ft.

Comments

This flight was a repeat of Flight 5, but with full tip tanks. Fuel stored in the tip ranks was not used during the flight. The offset of channel 7 noted after Flight 5 was reduced by demodulator balancing for this flight.

It was discovered upon analysis that large antisymmetric components were present in channel 8; a broken strain gauge was suspected.

Flight Number 7 — Date 28. 7. 67

Initial Fuel Condition	-	Full mains, empty tip tanks
Take off Weight	-	6, 877 lb.
Take off c. g. Positions	-	114. 51 inches aft of datum
Tasks Performed	-	4. 1
		4. 2 at 300 kts. I. A. S. and 5, 000 ft.

Comments

Smooth roller coasters without overloading the instrumentation were performed during this flight. Both single and multiple cycle roller coasters were performed with periods ranging from 10 seconds to 2 seconds using a simple manoeuvre director. The pilot was required to null the difference between demanded and measured centre of gravity acceleration.

Flight Number 8 — Date 18. 12. 67

Initial Fuel Condition	-	Full mains, empty tip tanks
Take off Weight	-	6, 877 lb.
Take of c. g. position	-	114. 51 inches aft of datum
Tasks Performed	-	4. 1
		4. 2 at 300 kts. I. A. S. and 6, 000 ft.

Comments

The object of this flight was to prove the rear spar load channel (channel 8) after replacing the strain gauges. The range of channel 7 was increased for this flight to overcome the offset problem.

Flight Number 9 — Date 15. 1. 68

Initial Fuel Condition	-	Full mains empty tip tanks.
Take off Weight	-	6, 877 lb.
Take off c. g. Position	-	114. 51 inches aft to datum

Tasks Performed - 4.1
4.3 at 300 kts. I.A.S. and 2,500 ft.
4.4 at 300 kts. I.A.S. and 2,500 ft.

Comments

Tasks 4.3 and 4.4 were performed in heavy turbulence. The pilot's acceleration meter recorded +3g, -1g during the flight and examination for possible damage was requested after the flight.

Flight Number 10 — Date 15. 1.68

Initial Fuel Condition	- Full mains, empty tip tanks
Take off weight	6877 lb.
Take off c.g. Position	114.51 inches aft of datum
Tasks Performed	4.1 4.3 at 300 kts. I.A.S. and 2,500 ft. 4.4 at 300 kts. I.A.S. and 2,500 ft.

Comments

This was a repeat of Flight Number 9 to ensure that tasks 4.3 and 4.4 had been accomplished successfully.

APPENDIX C

ANALYSIS THEORY

C.1 RECONSTITUTION OF THE VERTICAL COMPONENT OF GUST VELOCITY

The time histories of vane incidence, boom acceleration, and centre of gravity pitch rate were used to reconstitute the vertical component of gust velocity assuming:-

(i) Constant forward airspeed, i.e. the aircraft was presumed trimmed in steady level flight, and fore-and-aft aircraft motions about the steady state and fore-and-aft components of gust velocity were negligibly small.

(ii) Local pitch rate of the boom corresponded to that measured at the centre of gravity, i.e. elastic rotations of the fuselage about the transverse axis could be ignored.

(iii) Local roll rates of the boom could be neglected.

and (iv) Dynamic response of the vane could be ignored.

Using the notation of Figure 5, the incidence due to the vertical component of turbulence could be written

$$\frac{w}{V} = \beta + \int_o^t \left(\frac{\ddot{z}_v}{V} - \dot{\theta} \right) dt + C \qquad \text{C.1}$$

or

$$w = V_\beta + \int_o^t \left(z_v - V\dot{\theta} \right) dt + VC \qquad \text{C.2}$$

Where C was a constant of integration which, as only the dynamic component of gust velocity was required, could be ignored.

Equation C.2 was implemented as shown in Figure 5. It will be observed that inputs to the computer were, in effect, high pass filtered. This measure was taken to prevent very low frequencies and long term drifts of the replay system causing integrator overloads.

It is worth mentioning that replay speed adjustments required corresponding integrator time constant adjustments for the reconstitution to be correct.

C.2 COMPUTATION OF POWER SPECTRAL DENSITIES AND TRANSFER FUNCTIONS

Details of publications containing formal proofs of the fundamental relationships of power spectral analysis may be found in Reference 5. This section is concerned only with the implementation of these fundamental relationships.

Provided the excitation could be considered as random, continuous and stationary, then the power spectral density of the response of a system, $\phi_2(\omega)$, was related to the power spectral density of the excitation, $\phi_1(\omega)$, and the transfer function of the system, $T_{12}(i\omega)$, by the equation

$$\phi_2(\omega) = \left| T_{12}(i\omega) \right|^2 \phi_1(\omega) \qquad \text{C. 3}$$

Further, the cross spectral density of the response, $\phi_{12}(i\omega)$, relative in the input was

$$\phi_{12}(i\omega) = T_{12}(i\omega)\ \phi_1(\omega) \qquad \text{C. 4}$$

The mean square response of the output, $y_f(t)$, of a narrow bandpass filter having a transfer function $H(i\omega)$ could be written

$$\lim_{T\to\infty} \frac{1}{T} \int_0^T y_f^{\,2}(t)\ dt = \int_0^\infty \phi_2(\omega)\ d\omega \qquad \text{C. 5}$$

$$= \int_0^\infty \left| H(i\omega) \right|^2 \phi_1(\omega)\ d\omega \qquad \text{C. 6}$$

where $\phi_1(\omega)$ and $\phi_2(\omega)$ were signal power spectral densities before and after filtering, respectively.

If the bandwidth of the filter was such that $\phi_1(\omega)$ could be considered constant for a particular centre frequency, ω_o, then equation C. 6 could be written

$$\lim_{T\to\infty} \frac{1}{T} \int_0^T y_f^{\,2}(t)\ dt = \phi_1(\omega_o) \int_0^\infty \left| H(i\omega) \right|^2 d\omega \qquad \text{C. 7}$$

Equation C. 7 provided the means for determining directly the power spectral density of an analogue signal using a variable centre frequency narrow bandpass filter, a squaring device, and an integrator.

A technique for measuring the transfer function, $T_{12}(i\omega)$, relating one time history, $y_2(t)$, to another, $y_1(t)$, was deducted from the properties of the cross correlation function.

$$R_{12}(\tau) = \lim_{T\to\infty} \frac{1}{T} \int_{-T}^{T} y_1(t).\ \ y_2(t+\tau)\ dt \qquad \text{C. 8}$$

$$= \int_{-\infty}^{\infty} \exp\ (i\omega\tau)\ \ \phi_{12}(i\omega)\ d\omega \qquad \text{C. 9}$$

$$= \int_{-\infty}^{\infty} \exp\ (i\omega\tau)\ \ T_{12}(i\omega)\ \phi_1(\omega)\ d\omega \qquad \text{C. 10}$$

From equation C. 4. Moreover, if the time histories had previously been passed through two identical narrow bandpass filters of centre frequency, ω_o, equation C. 10 could be written

$$\lim_{T\to\infty} \frac{1}{T} \int_{-T}^{T} y_{f_1}(t).\ y_{f_2}(t+\tau)\ dt = R_e\{\exp(i\omega_o\tau)\ T_{12}(i\omega_o)\}\ \phi_1(\omega_o) \int_{-\infty}^{\infty} \left| H(i\omega) \right|^2 d\omega \qquad \text{C. 11}$$

following the same reasoning as that used to derive equation C. 7

It was of interest to note that the presence of uncorrelated noise in either data channel effected both power spectra, but not the corresponding cross spectral density. The noise level present was indicated by the coherence function defined as

$$\gamma(\omega) = \left|T_{12}(i\omega)\right| \cdot \left\{ \frac{\phi_1(\omega)}{\phi_2(\omega)} \right\} \qquad \text{C. 12}$$

Equation C. 11 provided a means for determining the transfer function since, using the properties of a transfer function,

$$\lim_{T\to\infty} \frac{1}{T}\int_0^T y_{f_1}(t)\, y_{f_2}(t)\, dt = {}_R T_{12}(i\omega_o)\, \phi_1(\omega_o) \int_0^\infty \left|H(i\omega)\right|^2 d\omega \qquad \text{C. 13}$$

and

$$\lim_{T\to\infty} \frac{1}{T}\int_0^T y_{f_1}(t)\, y_{f_2}\left(t - \frac{\pi}{2\omega_o}\right) dt = {}_I T_{12}(i\omega_o)\, \phi_1(\omega_o) \int_0^\infty \left|H(i\omega)\right|^2 d\omega \qquad \text{C. 14}$$

where

$$T_{12}(i\omega) = {}_R T_{12}(\omega) + i\, {}_I T_{12}(\omega) \qquad \text{C. 15}$$

or

$$ {}_R T_{12}(\omega_o) = \frac{1}{\phi_1(\omega_o) \int_0^\infty \left|H(i\omega)\right|^2 d\omega} \lim_{T\to\infty} \frac{1}{T}\int_0^T y_{f_1}(t)\, y_{f_2}(t)\, dt \qquad \text{C. 16}$$

and

$$ {}_I T_{12}(\omega_o) = \frac{+1}{\phi_1(\omega_o) \int_0^\infty \left|H(i\omega)\right|^2 d\omega} \lim_{T\to\infty} \frac{1}{T}\int_0^T y_{f_1}(t)\, y_{f_2}\left(t - \frac{\pi}{2\omega_o}\right) dt \qquad \text{C. 17}$$

Thus two variable centre frequency narrow bandpass filters, a ninety degree phase shifting device, two multipliers, and two integrators could be used to determine directly the transfer function relating two analogue signals.

A second order filter was chosen for the present analysis having a transfer function

$$H(i\omega) = \frac{i\omega}{(\omega_o^2 - \omega^2) + 2i\zeta\omega_o\omega} \qquad \text{C. 18}$$

The differential equation realising equation C. 18, written in terms of an input voltage V_i and an output voltage V_o is

$$\ddot{V}_o + 2\zeta\omega_o\dot{V}_o + \omega_o^2 V_o = V_i \qquad \text{C. 19}$$

It can be seen from equations C. 7, C. 16 and C. 17 that it was necessary to evaluate

$$K_o = \int_0^\infty |H(i\omega)|^2 \, d\omega \qquad \text{C. 20}$$

$$= \frac{\pi}{4 \zeta \omega_o} \qquad \text{C. 21}$$

A result readily achieved using Cauchy's Residue Theorem.

The time lag necessary to obtain the imaginary component of a transfer function, q. v. equation C. 17, was obtained using a unity gain phase shift network having a transfer function

$$T_{(90)}(i\omega) = \left\{ \frac{1 - i(\omega/\omega_o)}{1 + i(\omega/\omega_o)} \right\} \qquad \text{C. 22}$$

The integral equation realising equation C. 22 written in terms of an input voltage V_i and an output voltage V_o, was

$$V_o = \omega_o \int_{-\infty}^{t} (V_i - V_o)dt - V_i \qquad \text{C. 23}$$

A network for a power and cross spectral analyser utilising the results obtained in equations C. 7, C. 16, C. 17, C. 19 and C. 23 is shown in Figure 6. With the two pole switch shown in Figure 6 in position 1 it was possible to compute simultaneously the power spectral densities of both input signals, integrator 1 storing a signal proportional to the power spectral density of channel 1, and integrator 2 storing a signal proportional to the power spectral density of channel 2. The transfer function of channel 2 relative to channel 1 could be determined with the two pole switch in position 2. In this case a signal proportional to the real part of the transfer function was stored in integrator 1, whilst a signal proportional to an imaginary part of the transfer function was stored in integrator 2.

The closed loop configuration of the bandpass filters and the phase shift network allowed the use of inexpensive differential amplifiers as integrator elements in these circuits, offsets due to amplifier imperfections being balanced at the inputs to the integrators. Integrators 1 and 2 of Figure 6 were, of course, controlled and used high quality, drift corrected amplifiers. The largest source of inaccuracy in the analyser was drift within the multipliers, and to reduce the effect of this the output of each filter was optimised using a gain increasing amplifier.

C. 3 ESTIMATION OF DAMPING COEFFICIENTS

The effective in-flight damping coefficients of modes excited by turbulence could have been estimated from the transfer function of a suitable mode with respect to the turbulence. It proved difficult, however, to determine accurately the apparent increase in damping caused by bias errors occurring in cross spectral density estimates, and effective damping coefficients were therefore obtained from suitable power spectral density estimates.

Provided that modes were widely separated and the contribution of a particular mode to the acceleration power density at a point on the aircraft greatly exceeded the contributions of all other modes near its resonant frequency, the following relationship could be written.

$$(\omega_1^2 - \omega^2) + 4\zeta_1^2 \omega_1^2 \omega^2 = 4X\zeta_1^2 \omega_1^4 \qquad \text{C. 24}$$

where ω_1 was the natural frequency and ζ_1 the damping coefficient of the mode under consideration, and X was the ratio of the power density at frequency ω_1 and the power density at frequency ω

Equation C. 24 was solved to give

$$\omega^2 = \omega_1^2 \left\{ 1 - 2\zeta_1^2 \pm 2\zeta_1 (\zeta_1^2 + X - 1)^{\frac{1}{2}} \right\} \qquad \text{C. 25}$$

Writing $\Delta\omega_1$, $\Delta\omega_2$ as the frequency intervals between ω_1, and the two frequencies given by Equation C. 25, then

$$(\omega_1 + \Delta\omega_2)^2 - (\omega_1 - \Delta\omega_1)^2 = \omega_1^2 \, 4\zeta_1 (\zeta_1^2 + X - 1)^{\frac{1}{2}} \qquad \text{C. 26}$$

or

$$2\omega_1 (\Delta\omega_1 + \Delta\omega_2) + (\Delta\omega_1^2 - \Delta\omega_2^2) = 4\zeta_1\omega_1^2 (\zeta_1^2 + X - 1)^{\frac{1}{2}} \qquad \text{C. 27}$$

Provided that ζ_1 was small, $(\Delta\omega_1^2 - \Delta\omega_2^2)$ could be neglected. Writing

$$(\Delta\omega_1 + \Delta\omega_2) = \Delta\omega \qquad \text{C. 28}$$

Then Equation C. 27 became

$$\Delta\omega = 2\zeta_1\omega_1^2 (\zeta_1^2 + X - 1)^{\frac{1}{2}} \qquad \text{C. 29}$$

or, after some rearrangement

$$\zeta_1^2 = \frac{(1 - X)}{2} + \frac{1}{2}\left\{ (1 - X)^2 + \left(\frac{\Delta\omega}{\omega_1}\right)^2 \right\}^{\frac{1}{2}} \qquad \text{C. 30}$$

Assuming that $\frac{\Delta\omega}{\omega_1}$ was small, Equation C. 30 could be written

$$\zeta_1^2 \doteq \frac{1}{2}\left(\frac{\Delta\omega}{\omega_1}\right) \cdot \frac{1}{(X - 1)^{\frac{1}{2}}} \qquad \text{C. 31}$$

The above analysis assumed that no bias error was present in the power density. If an estimate of power density containing bias errors was to be used to estimate damping coefficient, then Equation C. 31 could be used provided that an equivalent value of X could be determined.

Suppose that the transfer function of the acceleration of a point on the aircraft to the turbulence could be written

$$T_{12}(i\omega) \propto \frac{-\omega^2}{(\omega_1^2 - \omega^2) + 2i\zeta_1\omega_1\omega} \qquad \text{C. 32}$$

Also, suppose that the turbulence power spectral density was approximately inversely proportional to the square of the frequency, then the estimated power spectral density of the acceleration of the point could be written

$$\bar{\phi}_1(\omega_o) \propto \int_0^\infty \frac{\omega^2}{\{(\omega_1^2 - \omega^2)^2 + 4\zeta_1^2\omega_1^2\omega^2\}} \; \frac{\omega^2}{\{(\omega_o^2 - \omega^2)^2 + 4\zeta^2\omega_o^2\omega^2\}} \cdot d\omega \qquad \text{C. 33}$$

Writing the natural frequency of the filter

$$\omega_o = \omega_1 (1 + \Delta) \qquad \text{C. 34}$$

and assuming Δ to be small, Equation C. 33 was evaluated to give

$$\bar{\phi}_1(\omega_o) \propto \frac{\pi}{16\omega_o^3\zeta\zeta_1} \cdot \left[\frac{(\zeta + \zeta_1)\{\Delta^2 + (\zeta_1 - \zeta)^2\}}{\Delta^4 + 2\Delta^2(\zeta^2 + \zeta_1^2) + (\zeta^2 - \zeta_1^2)^2} \right] \qquad \text{C. 35}$$

Equation C. 35 was used to determine the apparent power density ratio

$$\bar{X} = \frac{\phi_1(\omega_o)_{\Delta = o}}{\bar{\phi}_1(\omega_o)} = \frac{\Delta^4 + 2\Delta^2(\zeta^2 + \zeta_1^2) + (\zeta_1^2 - \zeta^2)^2}{(\zeta + \zeta_1)^2\{\Delta^2 + (\zeta_1 - \zeta)^2\}} \qquad \text{C. 36}$$

This was to be rearranged to give, for the particular case of $\overline{X} = 2$

$$\Delta = \zeta + \zeta_1 \qquad \text{C. 37}$$

It was noted that

$$\Delta = \frac{1}{2}\frac{\Delta\omega}{\omega_1} \qquad \text{C. 38}$$

and that, from Equation E. 6

$$\zeta = \frac{\Omega}{\pi\omega_1} \qquad \text{C. 39}$$

allowing Equation C. 37 to be written

$$\zeta_1 = \frac{1}{2}\left(\frac{\Delta\omega}{\omega_1}\right) - \frac{\Omega}{\pi\omega_1} \qquad \text{C. 40}$$

C. 4 ESTIMATION OF R. M. S. GUST VELOCITY

The high pass filtering used in the reconstitution of gust velocity precluded direct measurement of the root mean square value of the gust velocity. However and estimate of its value was obtained by assuming that the gust velocity obeyed the law

$$\phi(\omega) = \frac{\sigma^2 L}{\pi V} \left\{ \frac{1 + {}^8/3\ (1.339\ \omega L/V)^2}{[1 + {}^8/3\ (1.339\ \omega L/V)^2]^{11/6}} \right\} \qquad \text{C. 41}$$

At high frequencies, Equation C. 41 could be approximated by

$$\phi(\omega) \doteq \frac{0.5215}{\omega^{5/3}} \cdot \left(\frac{V}{L}\right)^{2/3} \cdot \sigma^2 \qquad \text{C. 42}$$

allowing an estimate of σ, the root mean square value of gust velocity, provided suitable values of V and L were assumed.

APPENDIX D

ANALYSIS EQUIPMENT AND PROCEDURE

D. 1 ANALYSIS EQUIPMENT

Flight recordings were replayed using a flexonics M400 magnetic tape deck whose speed could be controlled either by an internally generated reference frequency or by the 12KHz reference signal recorded on all flight magnetic tapes. Four Flexonics DFM4 discriminators were available for demodulating data channels, channel and discriminator selection being made via a "patch field". A feature of the discriminator was the amplified, but undiscriminated, output available for re-recording purposes.

Repetitive replaying of a sample of flight recording was facilitated by the use of a seven track magnetic tape loop device, Thermionic Products TLS2. A patch field and control panel for this machine were designed and constructed by the Department of Flight. Included in the control panel were three changeover relays, each operated by the rectified output from a high gain, narrow bandwidth 3KHz filter. The filters were designed so that the relays could be operated by head currents derived from 3KHz signals pre-recorded onto the tape loop. The tape loop was controlled by a short oxide-free section of magnetic tape actuating a photoelectric cell which, in turn, controlled the action of the start/stop relay. Restart was achieved by overriding the photoelectric cell circuit.

The scaling of discriminator outputs and computation of power and cross spectra were performed using an analogue computer designed and constructed by the Department of Flight. The computer was based upon commercially available ten volt solid state operational amplifiers, drift corrected for open loop integration but differential and of moderate gain elsewhere. The construction of an accurate multiplier posed a large problem; finally selected was a development of that described in Reference 4, using the mark-space ratio technique and having a gain of 0. 1. The computer could be controlled either internally, in the normal way, or remotely by connecting appropriate voltages to readily accessible control terminals.

A general view of the analysis equipment is shown in Figure 3, and a block diagram is displayed in Figure 4.

D. 2 ANALYSIS PROCEDURE

After a sample of flight recording had been chosen for analysis, up to four tracks of the selected sample were selected and each connected to a discriminator using the replay patch field, q. v. Figure 4. The re-record output from each discriminator was connected to a track of the tape loop deck via the tape loop patch field. Then with replay deck set to operate at $7\frac{1}{2}$ inches per second and the tape loop loaded with a clean magnetic tape loop of suitable length and set to operate at $3\frac{3}{4}$ inches per second, the chosen tracks were re-recorded onto the magnetic tape loop commencing 30 seconds before the start of the sample to allow time for initial transients in the analyser to decay.

Computer control signals were then recorded onto the magnetic tape loop using a stop watch and a 750 Hz oscillator set at a suitable output level and connected to a chosen track of the tape loop deck via an on/off switch. With the tape loop deck set to operate at $3\frac{3}{4}$ inches per second and the re-record outputs disconnected from the tape loop patch field, the tape loop was recycled with the output from the switch connected, in turn, to each of three tape loop tracks via the tape loop patch field. The oscillator was switched to the first track from the start of the settling period until two seconds or so after the end of the sample to provide a means of resetting the integrator used in the reconstitution of gust velocity and a means of switching out the analogue signals from the discriminators between tape loop cycles. The oscillator signal was switched to the second track from the start of the settling point until a second or so before the start of the sample to provide a means of resetting the analyser output integrators, and was switched to the third track for the duration of the sample to provide a means for switching the output of the multipliers to the output integrators.

The re-recorded time histories were next calibrated by replaying the calibration voltages recorded at the beginning of each flight, q.v. Reference 1, with the replay deck operating at 30 inches per second and the discriminators adjusted to have zero output for zero calibration volts.

Finally, with the gains of the discriminator buffer amplifiers and following potentiometers suitably set, the date channels re-recorded onto the magnetic tape loop connected to the appropriate discriminator, the filter switches connected to the correct tape loop track and to the correct control channel; and with the tape loop deck set to operate at 15 inches per second, the equipment was ready for spectral analysis of the chosen data tracks.

Centre frequency and bandwidth distributions used for the spectral analysis of the flight records are shown in Table 2.

During the analysis the outputs of both filters, both multipliers, and the phase shift network were checked before each cycle of the tape loop to ensure no output for a null input. The gains of each filter was separately adjusted, where necessary, to obtain maximum output without overload. At each frequency the tape loop was cycled twice, firstly with the two pole switch, shown in Figure 6, in position 1 to obtain, after a simple slide rule operation, the power spectral density of each channel, and secondly with the two pole switch in position 2 to obtain, again after a simple slide rule operation, the transfer function of the second data channel relative to the first.

Supposing the gain of data channel 1 to be X_1 units per volt, the gain of channel 2 to be X_2 units per volt, and the "real time" gain product of the first integrator and the output amplifier in the bandpass filters shown in Figure 6 to be G_1 and G_2 respectively, then the results of Appendix C were used to deduce that with the two-pole switch in position 1

$$\phi_1(\omega_o) = \left(\frac{X_1}{G_1}\right)^2 \cdot \frac{4\zeta\omega_o}{\pi T} \cdot K_1 \qquad \text{D. 1}$$

and

$$\phi_2(\omega_o) = \left(\frac{X_2}{G_2}\right)^2 \cdot \frac{4\zeta\omega_o}{\pi T} \cdot K_2 \qquad \text{D. 2}$$

where T represented the "real time" integration period in seconds, and where K_1 and K_2 represented the final voltages of integrators 1 and 2 respectively. With the two-pole switch in position 2

$$R^T{}_{12}(\omega_o) = \frac{X_1X_2}{G_1G_2} \cdot \frac{4\zeta\omega_o}{\pi T} \cdot \frac{K_1}{\phi_1(\omega_o)} \qquad \text{D. 3}$$

$$ {}_{I}T_{12}(\omega_o) = \frac{X_1 X_2}{G_1 G_2} \cdot \frac{4\zeta\omega_o}{\pi T} \cdot \frac{K_1}{\phi_1(\omega_o)} \qquad D.4 $$

It is worth noting that Equations D. 1 and D. 4 are valid for real time cycling of time histories. The equations remain valid for the procedure described above if the time constants of all analyser integrators are decreased by a factor of 4. If this procedure is not followed, then the correct result may be obtained from the network shown in Figure 6 by assuming, for setting up purposes only, that the centre frequency is four times that required, and by multiplying the results obtained from Equations D. 1 to D. 4 by 64.

APPENDIX E

ANALYSIS ERRORS

Errors in the experimental analysis arise both from the particular techniques employed and from the implementation of that technique. In the present case errors due to the technique arise from the finite filter bandwiths, termed bias errors, and from the finite length of samples analysed, termed variance errors.

E.1 BIAS ERRORS

Bias errors occur when the slope of the power spectral density varies with frequency. In order, therefore, to determine the magnitude of the bias error, the shape of the unbiased spectral density must be estimated. In the present case the greatest rate of change of slope of a power spectral density can be expected to occur close to a natural frequency of the aircraft. Furthermore, for a particular natural frequency, the greatest rate of change of slope occurs at measurement points where the aircraft can be considered to act as a single degree of freedom system. Assuming that the aircraft is excited by turbulence having a power spectral density inversely proportional to the square of the frequency, the power spectral density, $\phi(\omega)$, of the output from an accelerometer positioned at the critical position for a particular mode having a natural frequency ω_1 and damping ratio ζ_1 can be approximated by

$$\phi_1(\omega) \propto \frac{\omega^2}{(\omega_1^2 - \omega^2)^2 + 4\zeta_1^2\omega_1^2\omega^2} \qquad \text{E.1}$$

The bias error has been derived in Reference 2 as

$$\epsilon(\omega) = \frac{\Omega_e^2}{24} \cdot \frac{\phi_1''(\omega)}{\phi_1(\omega)} \qquad \text{E.2}$$

where Ω_e is the equivalent statistical bandwidth of the analyser filter. Using the power spectral density E.1 and assuming ζ_1 small,

$$\epsilon_{max} = \frac{\Omega_e^2}{24} \cdot \frac{\phi_1''(\omega_1)}{\phi_1(\omega_1)} \qquad \text{E.3}$$

i.e.

$$\epsilon_{max} = \frac{-\Omega_e^2}{24} \cdot \frac{2}{\omega_1^2\zeta_1^2} \qquad \text{E.4}$$

The equivalent statistical bandwidth of the filter having the transfer function defined by Equation C.18 has been computed in Reference 2 to be

$$\Omega_e = 2\Omega \qquad \text{E.5}$$

where

$$\Omega = 4\zeta^2\omega_o^2 \cdot \int_o^\infty |H(i\omega)|^2 d\omega = \pi\zeta\omega_o \qquad \text{E.6}$$

The derivation of Equation E.4 presumed a perfect "square window" filter whose bandwidth was sufficiently small for the power spectral density within the passband to be approximated by a four term Taylor series. The implication of this is that the bias error should be small for Equation E. 4 to be valid.

A more accurate expression for the maximum bias error in the estimate of a power spectral density similar to that of Equation E. 1 can be obtained by using the particular analyser filter characteristics. The computed power spectral density is

$$\bar{\phi}_1(\omega_o) \propto \frac{4\zeta\omega_o}{\pi}\int_o^\infty \frac{\omega^2}{\{(\omega_1^2-\omega^2)^2+4\zeta_1^2\omega_1^2\omega^2\}}\cdot\frac{\omega^2}{\{(\omega_o^2-\omega^2)^2+4\zeta^2\omega_o^2\omega^2\}}\,d\omega \qquad \text{E. 7}$$

Assuming ζ and ζ_1 to be small, and putting $\omega_1 = \omega_o$, Equation E. 7 may be evaluated to give

$$\phi_1(\omega_1) \propto \frac{1}{4\omega_1^2\zeta_1(\zeta+\zeta_1)} \qquad \text{E. 8}$$

Clearly, as $\zeta \to o$, Equation E. 8 reduces to

$$\phi_1(\omega_1) \propto \frac{1}{4\omega_1^2\zeta_1^2} \qquad \text{E. 9}$$

and the maximum bias error is given by

$$1 - \epsilon_{max} = \frac{\bar{\phi}_1(\omega_1)}{\phi_1(\omega_1)} = \frac{\zeta_1}{\zeta+\zeta_1} \qquad \text{E. 10}$$

$$\text{i. e.} \quad \epsilon_{max} = \frac{-\zeta}{\zeta+\zeta_1} \qquad \text{E. 11}$$

$$\text{or} \quad \epsilon_{max} = -\frac{\Omega}{\omega_1}\,\frac{1}{\left(\frac{\Omega}{\omega_1}+\pi\zeta_1\right)} \qquad \text{E. 12}$$

Maximum bias errors, obtained using effective damping coefficients computed from Equation C. 40, are shown in Table 4.

The bias errors in estimates of the power spectral density of atmospheric turbulence may be obtained by evaluating

$$\bar{\phi}_1(\omega_o) \propto \frac{4\zeta\omega_o}{\pi}\cdot\int_o^\infty\frac{1}{\omega^2}\cdot\frac{\omega^2}{(\omega_o^2-\omega^2)^2+4\zeta^2\omega_o^2\omega^2}\,d\omega \qquad \text{E. 13}$$

$$\propto \frac{1}{\omega_o^2} \qquad \text{E. 14}$$

Clearly, provided that the power spectral density of turbulence is nearly inversely proportional to the square of frequency, estimates of the power spectral density contain no bias error.

E. 2 VARIANCE ERRORS

Variance errors are shown in Reference 2 to be given by

$$\epsilon_{var} = \left(\frac{2\pi}{\Omega_e T} \right)^{\frac{1}{2}} \qquad \text{E. 15}$$

or

$$\epsilon_{var} = \left(\frac{\pi}{\Omega T} \right)^{\frac{1}{2}} \qquad \text{E. 16}$$

Variance error distributions for the present analysis are shown in Table 5.

E. 3 IMPLEMENTATION ERRORS

The implementation gave rise to three types of error. They were:

E. 3. 1 Scale Errors caused by inaccuracies in the instrumentation and and their ground calibrations, record and replay gain variations, and inaccuracies in the analysis computer.

E 3. 2 Variance Errors due to the inaccurate setting of the filters, to the presence of filter transients, and to zero offsets in the multipliers. Filter transients were presumed to be excited only by the start of the sample, and their contribution to the variance error was reduced to negligible proportions by the thirty second settling period allowed before commencement of integration. The effect of multiplier zero offset was minimised by scaling the voltage levels in the computer to be of maximum value without causing overloads. It should be noted, however, that multiplier offsets could seriously affect the accuracy of cross spectral density estimates when the appropriate values of coherence functions were small.

E 3. 3 Errors Due to Extraneous Noise were found to be significant at small values of power density. Flight recordings in fact contained extremely low levels of extraneous noise, but the process of re-recording the data onto a magnetic tape loop introduced "drop outs" of signal which appeared as large amplitude pulses in the output.

Estimates for the values of implementation errors are shown in Table 6.

APPENDIX F

AIRCRAFT STABILITY AND CONTROL DERIVATIVES

F.1 BASIC DATA

Assumed forward airspeed, 300 kts. I.A.S.	515 ft./sec. T.A.S.
Assumed air density at 3,000 ft.	.002177 slugs/cu.ft.
Dynamic pressure	289 lb./sq.ft.
Gross wing area	198 sq.ft.
Wing span	31.8 ft.
Wing mean chord	6.23 ft.
Tail arm ($\frac{1}{4}\ \bar{c}_w$ to $\frac{1}{4}\ \bar{c}_t$)	16.08 ft.
Gross tailplane area	31.85 sq.ft.
Tailplane span	10.56 ft.
Tailplane mean chord	3.02 ft.
Initial aircraft weight	6877 lb.
Initial c.g. position aft of transverse datum	114.51 in.
Measured aircraft pitching inertia	6900 slugs ft^2

F.2 TIP TANKS EMPTY

Assuming 300 litres of fuel used, an average condition for the analysed records,

Aircraft weight was	6407 lb.
c.g. position aft of transverse datum	114.25 in.
c.g. position ahead of wing $\frac{1}{4}\bar{c}$ position	0.15 in.
Lift coefficient, C_L	0.113
Deduced drag coefficient, C_D	0.022
Wing Lift curve slope, from M.S. data, $\partial C_L/\partial\alpha$	4.58 per rad.
Drag curve slope, from M.S. data, $\partial C_D/\partial\alpha$	.0655 per rad.
Tailplane lift curve slope, from C.o.A. data $\partial C_{L_t}/\partial\alpha$	4.30

Quasi-static stability derivatives were computed from the above data and from flight test measurements. The conventional British notation is used below.

x_u	-0.0221
z_u	-0.113
m_u	0
x_w	0.0238

z_w	-2.301
m_w	-0.0867
$m_{\dot{w}}$	-0.00456
x_q	0
z_q	-0.346
mq	-0.346
x_η	0
z_η	-0.173
m_η	-0.173
μ_1	28.8
t	0.898
i_B	0.1371

The equations of motion in still air were thus, <u>in real time,</u>

$$
\begin{array}{llll}
(D+0.0246)\bar{u} & -0.0265\ \bar{w} & +0.0629\ \theta = & 0 \\
0.126\ \bar{u} & +(D+2.562)\bar{w} & -0.988D\ \theta = & 0.1926\eta \\
 & (1.085D+22.16)\bar{w} & +(D^2+2.811D)\theta = & 45.0\eta
\end{array}
$$

giving a short period of natural frequency 0.86 Hz and damping ratio 0.595, and a phugoid of natural frequency 0.01238 Hz and damping ratio 0.153.

F.3 TIP TANKS FULL

Assuming 300 litres of main tank fuel used,

Aircraft weight was	7143 lb.
c.g. position aft of transverse datum	113.9 in.
c.g. position ahead of wing $\frac{1}{4}\bar{c}$ position	0.5 in.
Lift coefficient, C_L	0.120
Deduced drag coefficient, C_L	0.0222

Quasi-static stability derivatives were computed for this case as

x_u	-0.0222
z_u	-0.120
m_u	0
x_w	0.0253
z_w	-2.301

m_w	-0.0867
$m_{\dot{w}}$	-0.0041
x_q	0
z_q	-0.346
m_q	-0.346
x_η	0
z_η	-0.173
m_η	-0.173
μ_1	32.07
$\hat{t}$	1.00
i_B	.1241

The equations of motion were thus, <u>in real time,</u>

$$
\begin{array}{llllll}
(D+0.0222)\bar{u} & -0.0253\,\bar{w} & +0.06\theta & = & 0 \\
0.12\bar{u} & +(D+2.301)\bar{w} & -0.988\,\Delta\theta & = & .173\,\eta \\
 & +(1.059D+22.40)\bar{w} & +(D^2+2.798D)\theta & = & -44.70\,\eta
\end{array}
$$

Giving a short period of natural frequency 0.85Hz and damping ratio 0.573, and a phugoid of natural frequency .012Hz and damping ratio 0.143.

MAGNETIC TAPE TRACK NUMBER	QUANTITY MEASURED	TRANSDUCER TYPE	CALIBRATION UNITS PER VOLT RECORDED
1	Vane Incidence	R.A.E. Vane Inductive Pick Off Type 08/L4FLA	3.3 Degrees
2	Boom Acceleration	Electro Mechanism Type MEM 348	4.4 g
3	c.g. Pitch Rate	Smiths Gyro Type LS/IC/SI/2227	3.0 Deg/sec
4	c.g. Acceleration	Inductive Type Designed by R.A.E.	0.82 g
5	T/P Tip Acceleration	2 Paired R.A.E. Type ITI-22-F31	8.75 g
6	12 KHz Reference	-	-
7	T/P Total Load	Strain Gauge Bridges	301 LB.
8	T/P Rear Spar Load	Strain Gauge Bridge	264 LB.
9	Elevator Velocity	R.A.E. Type IR3-6-40	21.3 Deg/sec
10	Wingtip Acceleration	R.A.E. Type ITI-22-F31	4.09 g
11	Rear Fuselage Acceleration	R.A.E. Type ITI-22-F31	2.46 g
12	c.g. Acceleration	As for Track 4	0.82 g
13	Elevator Hinge Moment	Strain Gauge Bridge	50.5 LB.FT.
14	Speech	-	-

TABLE 1 SUMMARY OF INSTRUMENTATION

Centre Frequency Range (Hz)	Bandwidth and Centre Frequency Interval (Hz)	Analyser Scale Factor x Integration Time
0. 1 - 1. 0	0. 1	1. 02
1. 2 - 3. 0	0. 2	2. 04
3. 5 - 10. 5	0. 5	5. 10
11 - 20	1. 0	10. 20

TABLE 2 CENTRE FREQUENCY AND BANDWIDTH DISTRIBUTION

Description	Tip Tanks Full				Tip Tanks Empty			
	Resonance Test		Flight Test		Resonance Test		Flight Test	
	fo	ζ	fo	ζ	fo	ζ	fo	ζ
Short Period	-	-	0.85	0.594	-	-	0.86	0.576
Wing Bending	5.38	0.012	5.16	0.065	9.95	0.015	10.10	0.104
Wing Torsion	12.70	0.013	12.80	0.058	25.70	0.033	-	-
Fuselage Bending	15.10	0.021	15.10	0.062	15.00	0.020	15.10	0.048
Tailplane Bending	27.50	0.031	-	-	27.70	0.017	-	-

TABLE 3 SUMMARY OF MODES

Description of Mode	Maximum Bias Error (Per Cent)	
	Flight 6	Flight 9
Short Period	5.6	5.9
Wing Bending	32.0	13.1
Wing Torsion	-	-
Fuselage Bending	26.8	30.5
Tailplane Bending	-	-

TABLE 4 MAXIMUM BIAS ERRORS

Centre Frequency Range (Hz)	Variance Error (Per Cent)	
	Hands Off Samples	Hands On Samples
0.1 - 1.0	28.8	18.2
1.2 - 3.0	14.4	9.1
3.5 - 10.5	5.8	3.7
11.0 - 20.0	2.9	1.8

TABLE 5 VARIANCE ERRORS

	Description of Source	Estimated Error (Per Cent)
SCALE ERRORS	CALIBRATIONS	
	a) for Tailplane total load	4.0
	b) for Tailplane rear spar load	6.0
	c) for other channels	1.0
	RECORD/REPLAY	1.0
	COMPUTER SCALING	2.0
VARIANCE ERRORS	FILTER TRANSIENTS	0
	ANALYSIS FILTERS	2.0
	MULTIPLIER DRIFT	7.0
	SPURIOUS NOISE	NOT KNOWN

TABLE 6 IMPLEMENTATION ERRORS

FREQUENCY (Hz.)	INERTIA MATRIX ($slugs. ft.^2$)			
9.92	9.388	0.080	-0.125	-0.210
15.00	0.080	4.719	-1.917	0.318
25.70	-0.125	-1.917	13.791	0.374
27.70	-0.210	0.318	0.374	1.542

TABLE 7. INERTIA MATRIX, TIP TANKS EMPTY

FREQUENCY (Hz.)	INERTIA MATRIX (slugs. ft.^{2})			
5.38	27.083	5.312	-0.805	0.698
12.70	5.312	73.470	0.800	0.156
15.20	-0.805	0.800	6.521	0.292
27.50	0.698	0.156	0.292	1.778

TABLE 8 INERTIA MATRIX, TIP TANKS FULL.

			MODE SHAPES.			
	X ORD. ft.	Y ORD. ft.	MODE 1 (9.92 Hz)	MODE 2 (15.0 Hz)	MODE 3 (25.7 Hz)	MODE 4 (27.7 Hz)
Wing Deflections	12.05	3.94	0.020	-0.083	0.221	0.012
	12.03	4.94	0.041	-0.075	0.338	0.030
	11.99	5.94	0.106	-0.067	0.541	0.054
	11.97	6.94	0.178	-0.055	0.698	0.072
	11.95	7.94	0.257	-0.043	0.801	0.085
	11.92	8.94	0.343	-0.024	0.870	0.092
	11.90	9.94	0.439	-0.001	0.933	0.095
	11.88	10.94	0.545	0.018	0.960	0.095
	11.85	11.94	0.649	0.042	0.974	0.090
	11.82	12.94	0.769	0.067	0.991	0.079
	11.80	13.94	0.889	0.097	0.995	0.067
	11.79	14.90	1.000	0.127	1.000	0.050
Wing Rotations	12.05	3.94	-0.0006	0.0040	-0.121	0.004
	12.03	4.94	-0.0035	0.0041	-0.175	0.001
	11.99	5.94	-0.0116	0.0039	-0.265	-0.007
	11.97	6.94	-0.0141	0.0033	-0.344	-0.013
	11.95	7.94	-0.0182	0.0030	-0.414	-0.019
	11.92	8.94	-0.0212	0.0021	-0.481	-0.025
	11.90	9.94	-0.0230	0.0024	-0.549	-0.029
	11.88	10.94	-0.0243	0.0243	-0.615	-0.034
	11.85	11.94	-0.0235	0.0022	-0.676	-0.044
	11.82	12.94	-0.0241	0.0026	-0.759	-0.047
	11.80	13.94	-0.0262	0.0021	-0.856	-0.054
	11.79	14.90	-0.0231	0.0006	-0.951	-0.060
Tailplane Deflections	26.21	0	-0.190	0.527	-0.122	-0.221
	26.21	0.833	-0.192	0.557	-0.140	-0.179
	26.21	1.833	-0.198	0.622	-0.171	-0.029
	26.21	2.833	-0.208	0.733	-0.311	0.258
	26.21	3.833	-0.216	0.864	-0.519	0.611
	26.21	4.790	-0.224	1.000	-0.721	1.000
Tailplane Rotations	26.21	0	0.0086	-0.0410	0.011	0.0056
	26.21	0.833	0.0096	-0.0500	0.037	0.0013
	26.21	1.833	0.0073	-0.0540	0.059	-0.0244
	26.21	2.833	0.0110	-0.0661	0.103	-0.0907
	26.21	3.833	0.0051	-0.0702	0.128	-0.1520
	26.21	4.790	0.0012	-0.0707	0.106	-0.2830
Fuselage Deflections	-10.24	0	-0.059	2.080	0.171	0.276
	-4.15	0	-0.069	0.425	-0.027	-0.057
	1.02	0	-0.094	0.100	-0.005	0
	15.13	0	-0.082	-0.064	-0.028	-0.055
	27.23	0	-0.208	0.553	-0.125	-0.250

TABLE 9. MEASURED MODE SHAPES, TIP TANKS EMPTY

Note. Y ordinates are specified relative to the transverse datum and are positive if aft. Rotations are about the Y axis, and are positive if "nose up." Deflections are positive if upwards.

	X ORD. ft.	Y ORD. ft.	MODE SHAPES. MODE 1 (5.38 Hz)	MODE 2 (12.7 Hz)	MODE 3 (15.2 Hz)	MODE 4 (27.5 Hz)
Wing Deflections	12.05	3.94	-0.103	0.005	-0.096	-0.021
	12.03	4.94	-0.055	0.039	-0.092	-0.031
	11.99	5.94	0	0.059	-0.089	-0.041
	11.97	6.94	0.068	0.035	-0.084	-0.051
	11.95	7.94	0.147	0.030	-0.075	-0.058
	11.92	8.94	0.216	0.016	-0.066	-0.063
	11.90	9.94	0.346	-0.014	-0.056	-0.062
	11.88	10.94	0.458	0.004	-0.038	-0.058
	11.85	11.94	0.589	0.016	-0.015	-0.051
	11.82	12.94	0.724	0.018	0.023	-0.040
	11.80	13.94	0.852	0.022	0.051	-0.023
	11.79	14.90	1.00	0.026	0.079	-0.008
Wing Rotations	12.05	3.94	-0.003	0.065	0.024	0.0183
	12.03	4.94	0.001	0.110	0.024	0.0242
	11.99	5.94	0	0.174	0.023	0.0302
	11.97	6.94	0	0.244	0.022	0.0362
	11.95	7.94	-0.004	0.300	0.020	0.0405
	11.92	8.94	-0.001	0.358	0.017	0.0435
	11.90	9.94	0.003	0.434	0.015	0.0445
	11.88	10.94	0.005	0.494	0.009	0.0440
	11.85	11.94	0.002	0.564	0.002	0.0393
	11.82	12.94	0.003	0.657	-0.010	0.0329
	11.80	13.94	0.012	0.768	-0.020	0.0219
	11.79	14.90	0.026	0.885	-0.031	0.0109
Tailplane Deflections	26.21	0	-0.281	0.728	0.577	-0.210
	26.21	0.833	-0.281	0.741	0.606	-0.171
	26.21	1.833	-0.291	0.779	0.665	0.026
	26.21	2.833	-0.298	0.839	0.766	0.299
	26.21	3.833	-0.306	0.910	0.877	0.662
	26.21	4.790	-0.317	1.000	1.000	1.000
Tailplane Rotations	26.21	0	0.0055	-0.036	-0.0407	-0.0019
	26.21	0.833	0.0046	-0.034	-0.0499	-0.0042
	26.21	1.833	0.0161	-0.035	-0.0596	-0.0653
	26.21	2.833	0.0063	-0.034	-0.0791	-0.0980
	26.21	3.833	0.0112	-0.032	-0.0824	-0.1541
	26.21	4.790	0.0091	-0.034	-0.0719	-0.1927
Fuselage Deflections	-10.24	0	-0.145	-0.202	2.230	0.426
	-4.15	0	-0.109	0.009	0.488	-0.096
	1.02	0	-0.109	0.074	0.150	-0.017
	15.13	0	-0.167	0.214	-0.066	-0.073
	27.23	0	-0.300	0.794	0.675	-0.257

TABLE 10. MEASURED MODE SHAPES, TIP TANKS FULL.

Note. Y ordinates are specified relative to the transverse datum and are positive if aft. Rotations are about the Y axis, and are positive if "nose up". Deflections are positive if upwards.

STATION	Y (ft.)	MASS (slugs)	C.G. POSITION (ft. fwd. of ref. axis)	PITCH INERTIA ABOUT LOCAL C.G. (slugs. ft ^{2})
1	2.918	3.161	1.250	12.840
2	4.410	2.161	1.229	8.190
3	5.840	3.642	1.190	12.910
4	7.500	1.469	1.150	44.780
5	9.160	1.348	1.033	4.025
6	10.820	1.230	0.935	3.362
7	12.500	1.118	0.884	2.765
8	14.170	1.000	0.859	2.240
tip tanks empty:-				
9	15.820	1.801	1.791	
tip tanks full:-				
9	15.820	7.200	2.018	19.500

TABLE 11. ESTIMATED WING WEIGHT DISTRIBUTION.
(One side only)

STATION	X (ft. aft of datum)	MASS (slugs)
1	-2. 590	12. 186
2	0. 653	13. 038
3	3. 901	24. 326
4	6. 915	18. 857
5	9. 653	40. 194
6	13. 625	32. 919
7	17. 120	6. 206
8	20. 543	2. 109
9	24. 073	3. 259
10	26. 399	2. 860

TABLE 12. ESTIMATED FUSELAGE WEIGHT DISTRIBUTION

STATION	Y (ft.)	MASS (slugs)	C.G. POSITION (ft. fwd. of ref. axis)	PITCH INERTIA ABOUT LOCAL C.G. (slugs. ft.^{2})
1	0	0.1910	0.633	0.2126
2	0.312	0.1988	0.608	0.2140
3	0.936	0.1879	0.550	0.1884
4	1.561	0.1754	0.491	0.1624
5	2.182	0.1646	0.437	0.1361
6	2.810	0.1512	0.379	0.1122
7	3.435	0.1413	0.321	0.0923
8	4.060	0.1289	0.266	0.0764
9	4.690	0.1538	0.208	0.0764
10	5.290	0.2163	0.167	0.0784

TABLE 13. ESTIMATED TAILPLANE + ELEVATOR WEIGHT DISTRIBUTION

(one side only)

POINT	CO-ORDINATES REL. TRANSVERSE DATUM (POSITIVE AFT)	
	X ORDINATE ft.	Y. ORDINATE ft.
A	-10.24	0
B	-4.15	0
C	0	0
D	7.45	2.033
E	7.45	0
F	12.12	0
G	14.59	0
H	14.59	2.033
J	24.06	0
K	26.21	0
L	27.72	1.56
M	27.72	0
N	6.02	15.86
O	8.87	15.86
P	11.75	15.86
Q	13.69	15.86
R	14.12	17.08
S	14.62	17.08
T	15.09	15.86
U	25.07	4.84
V	25.27	5.22
W	26.21	5.54
X	27.40	5.69

TABLE 14. CO-ORDINATES OF LABELLED POINTS IN FIGURE 2

FIGURE 1. M.S. 760 'PARIS' AIRCRAFT

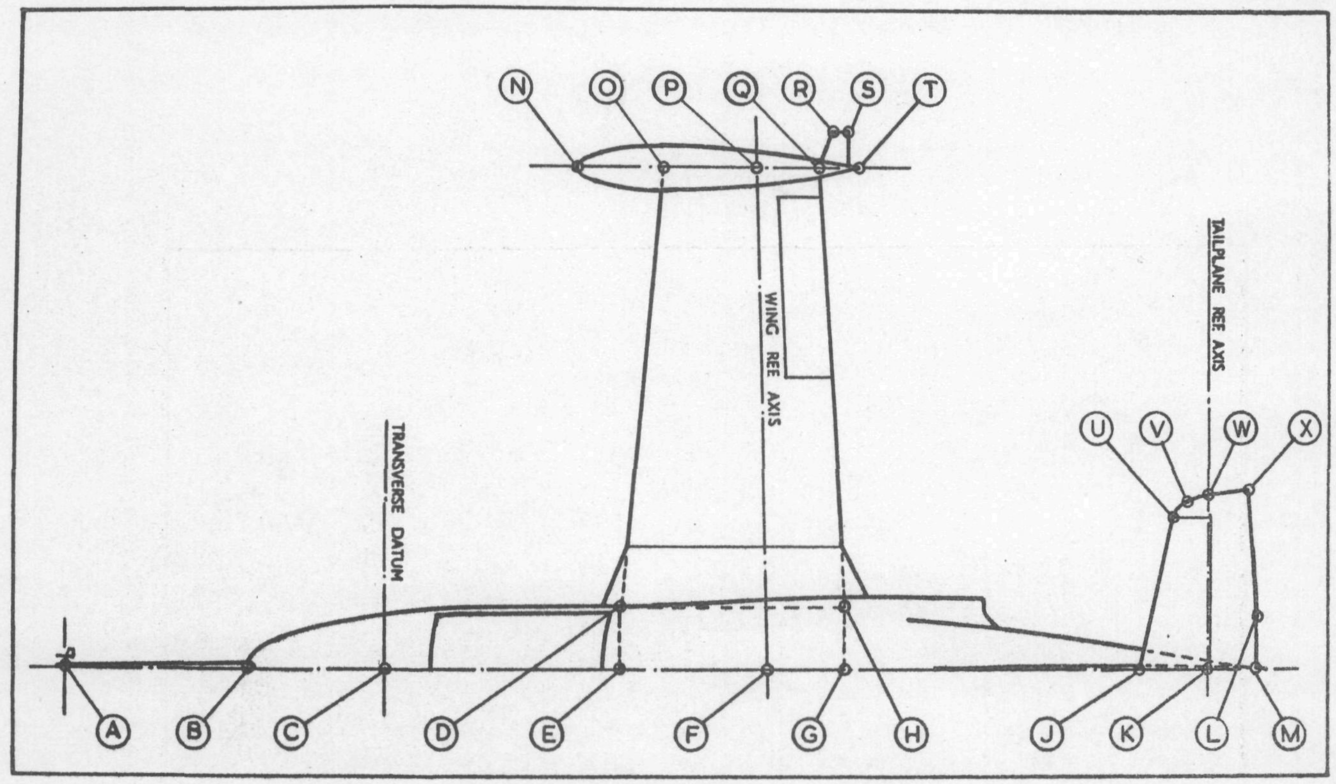

FIGURE 2. AIRCRAFT GEOMETRY

(COORDINATES OF LABELLED POINTS ARE LISTED IN TABLE 14, REL. TRANSVERSE DATUM)

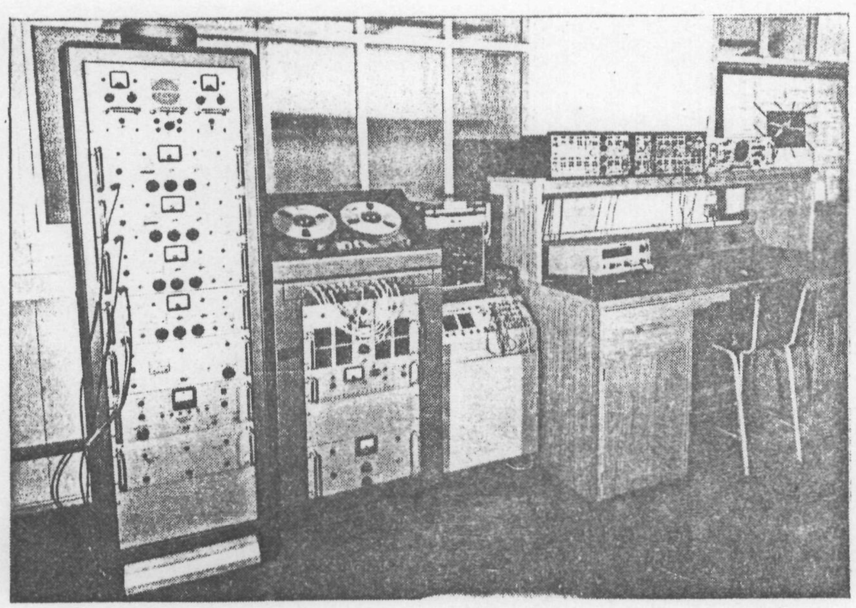

FIGURE 3. GENERAL VIEW OF ANALYSIS EQUIPMENT

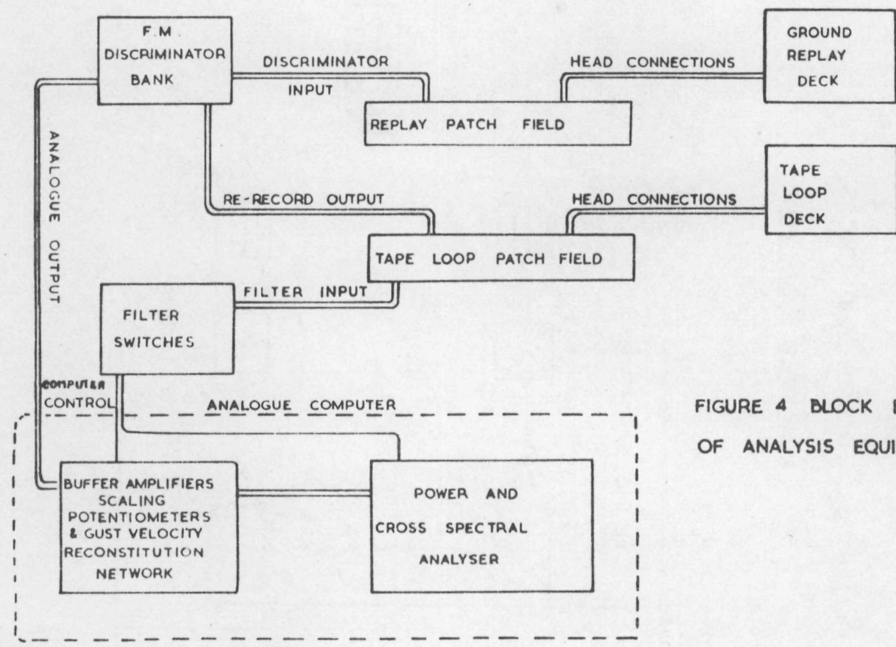

FIGURE 4 BLOCK DIAGRAM OF ANALYSIS EQUIPMENT

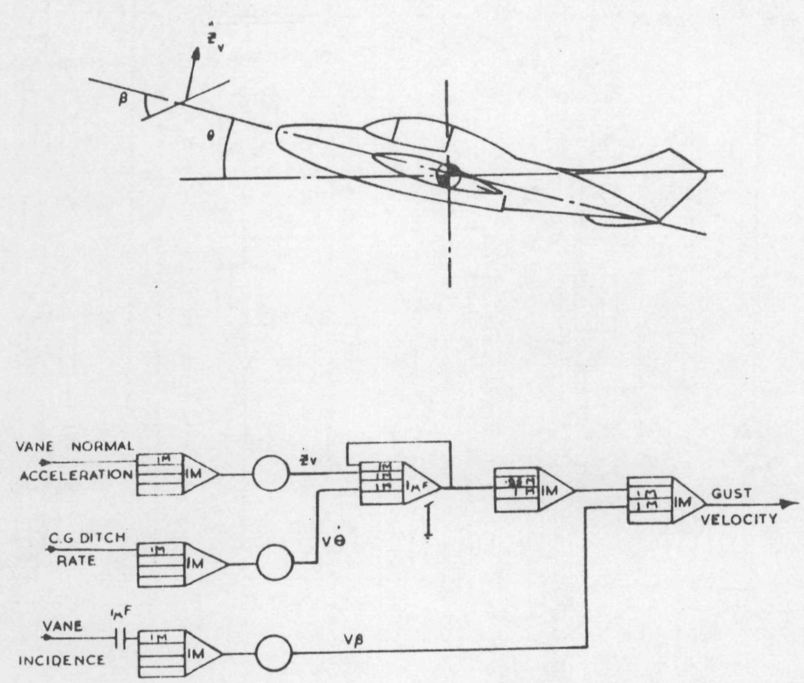

FIGURE 5 RECONSTITUTION OF VERTICAL COMPONENT OF GUST VELOCITY

FIGURE 6 POWER AND CROSS SPECTRAL ANALYSER

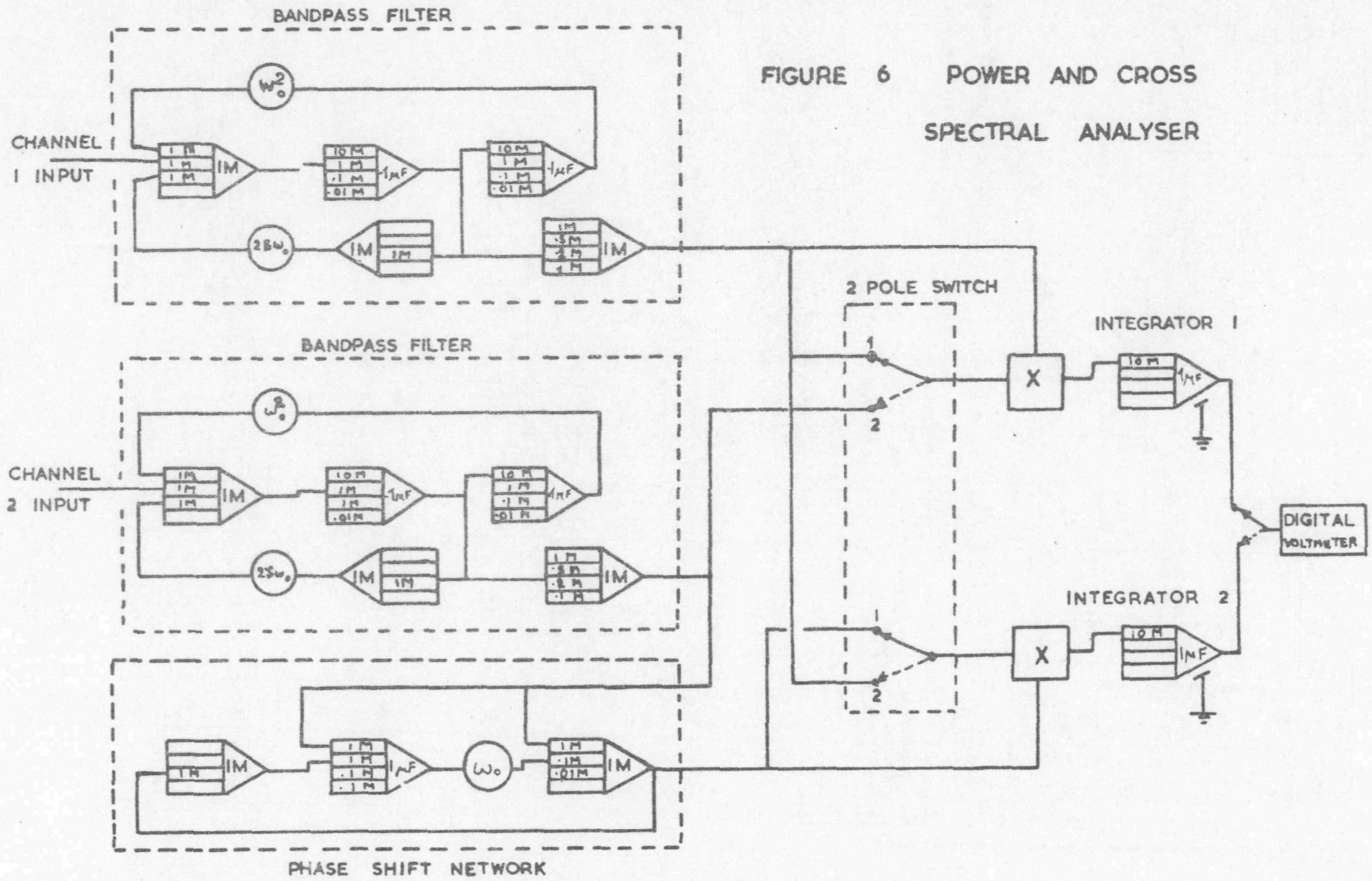

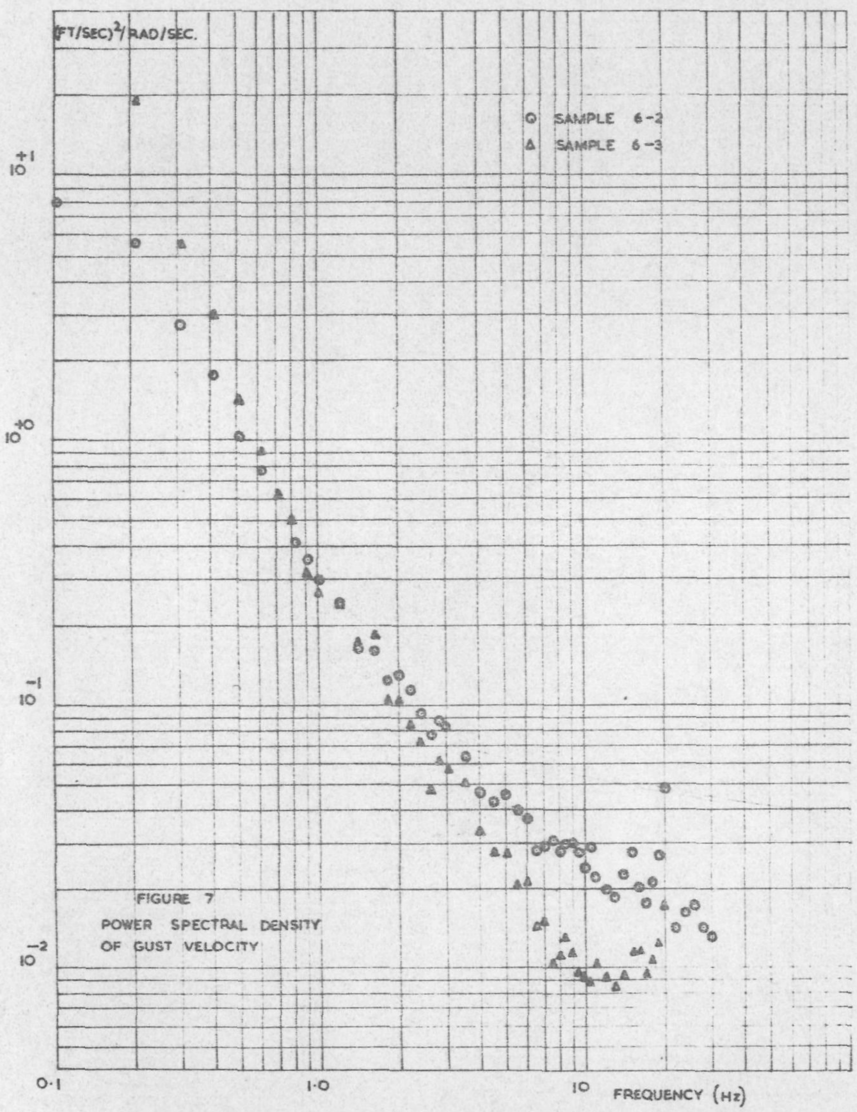

FIGURE 7 POWER SPECTRAL DENSITY OF GUST VELOCITY

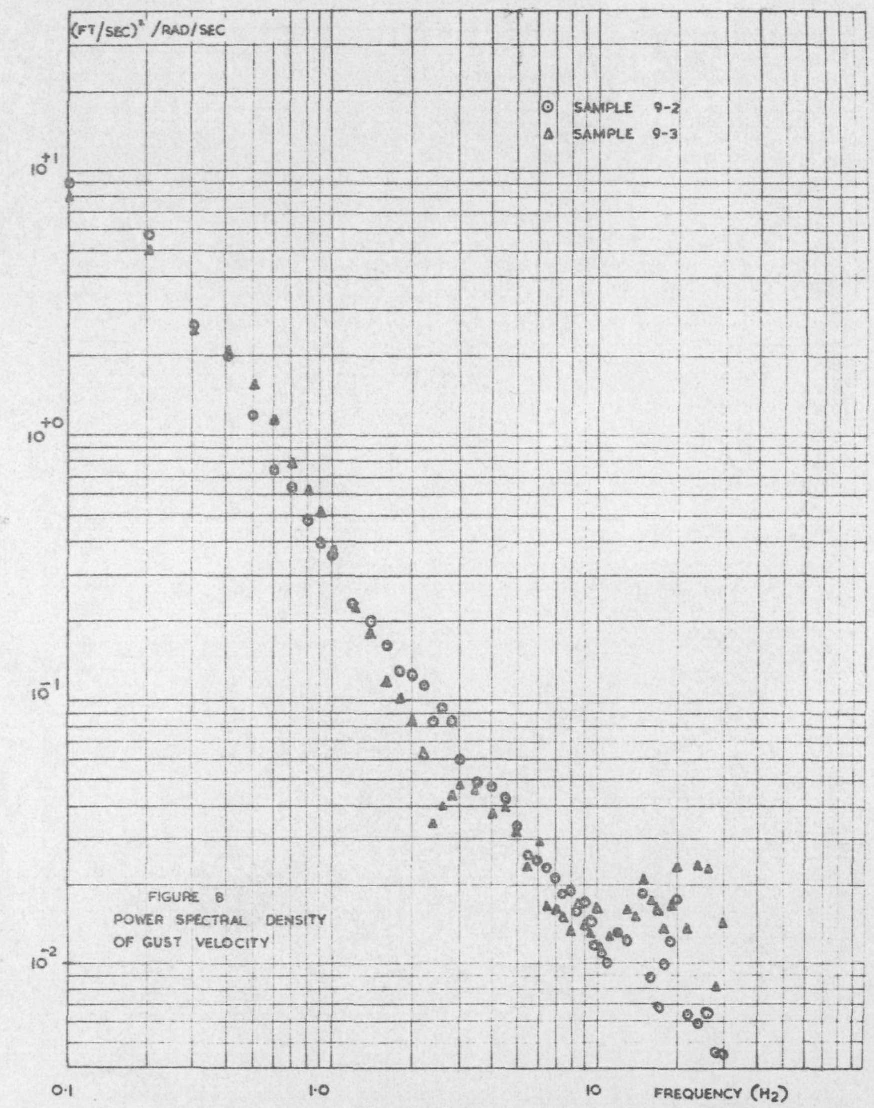

FIGURE 8 POWER SPECTRAL DENSITY OF GUST VELOCITY

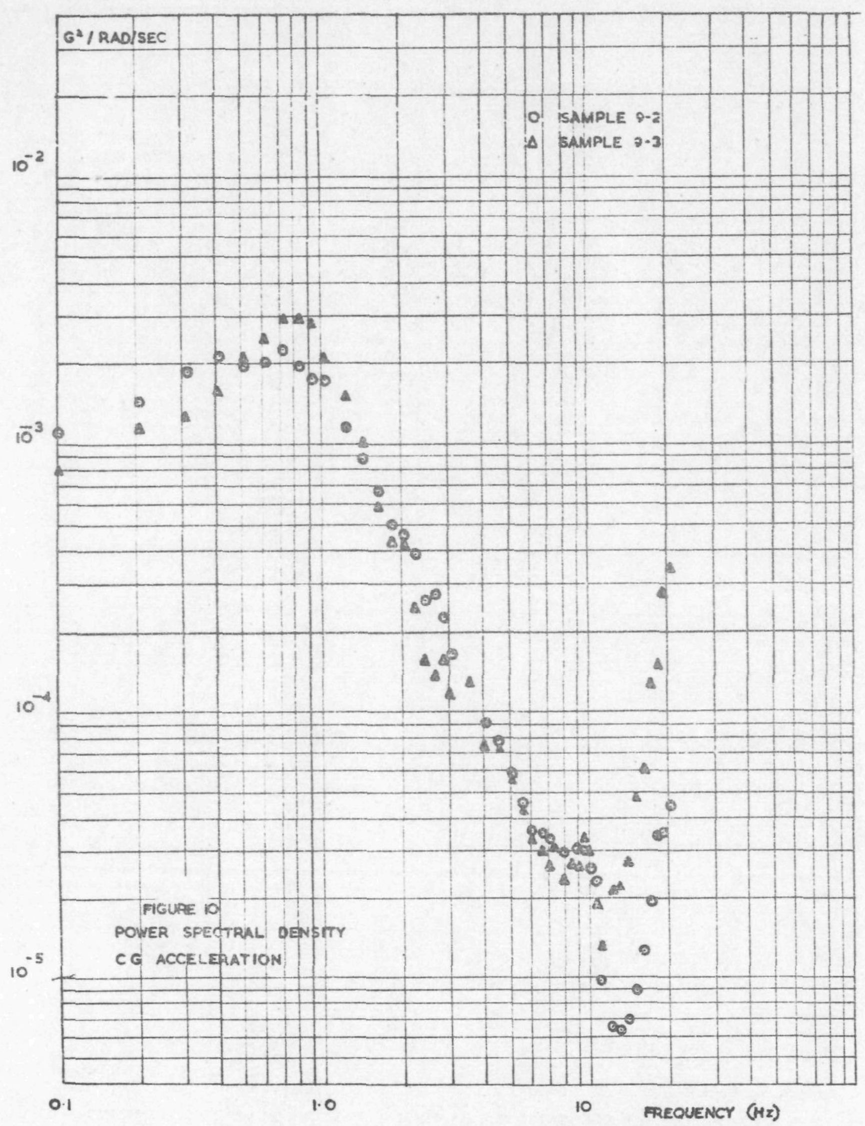

FIGURE 10 POWER SPECTRAL DENSITY C G ACCELERATION

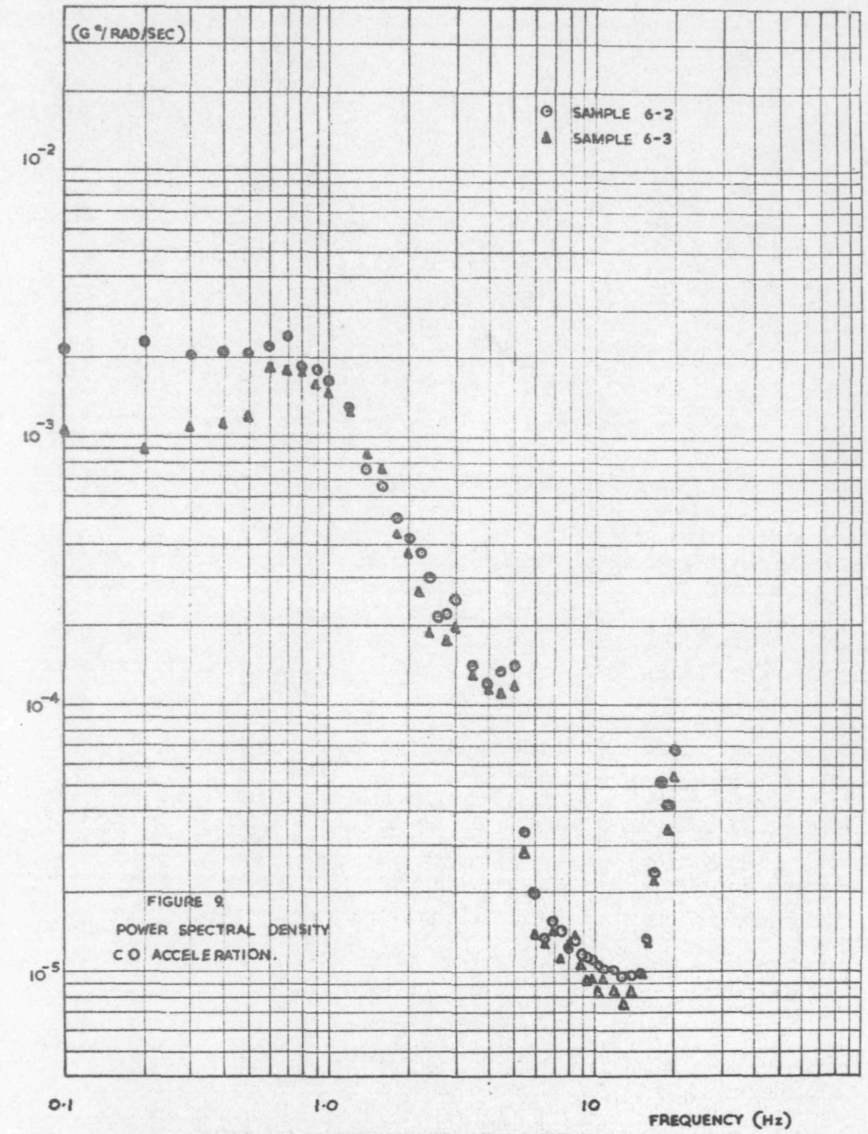

FIGURE 9 POWER SPECTRAL DENSITY C O ACCELERATION

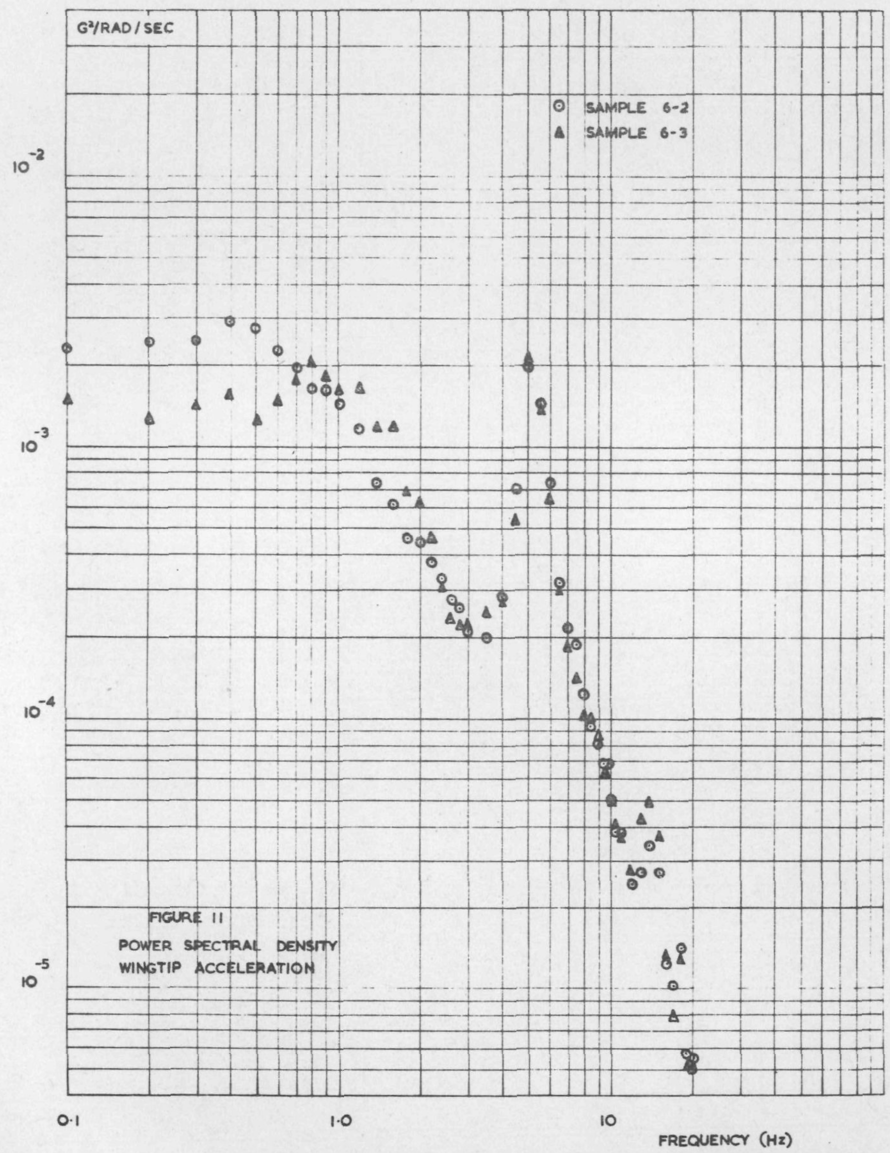

FIGURE 11 POWER SPECTRAL DENSITY WINGTIP ACCELERATION

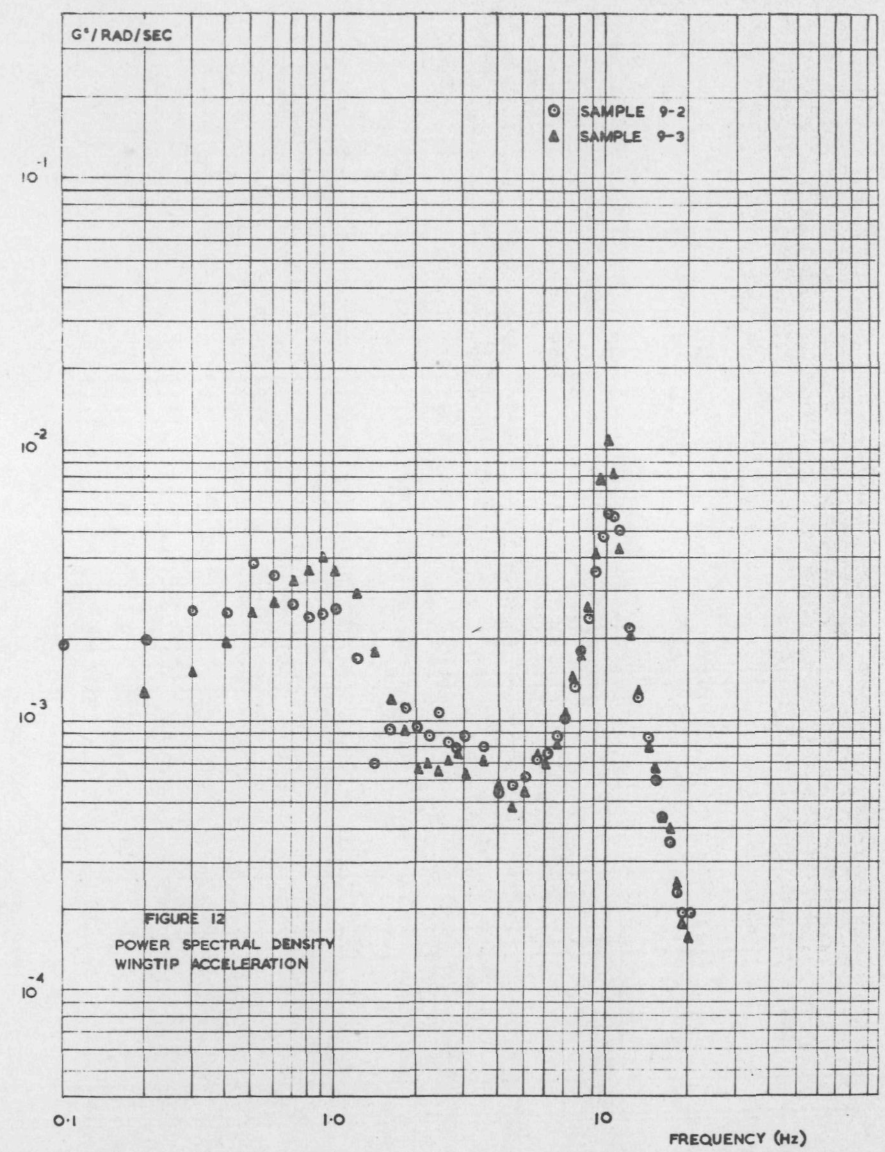

FIGURE 12 POWER SPECTRAL DENSITY WINGTIP ACCELERATION

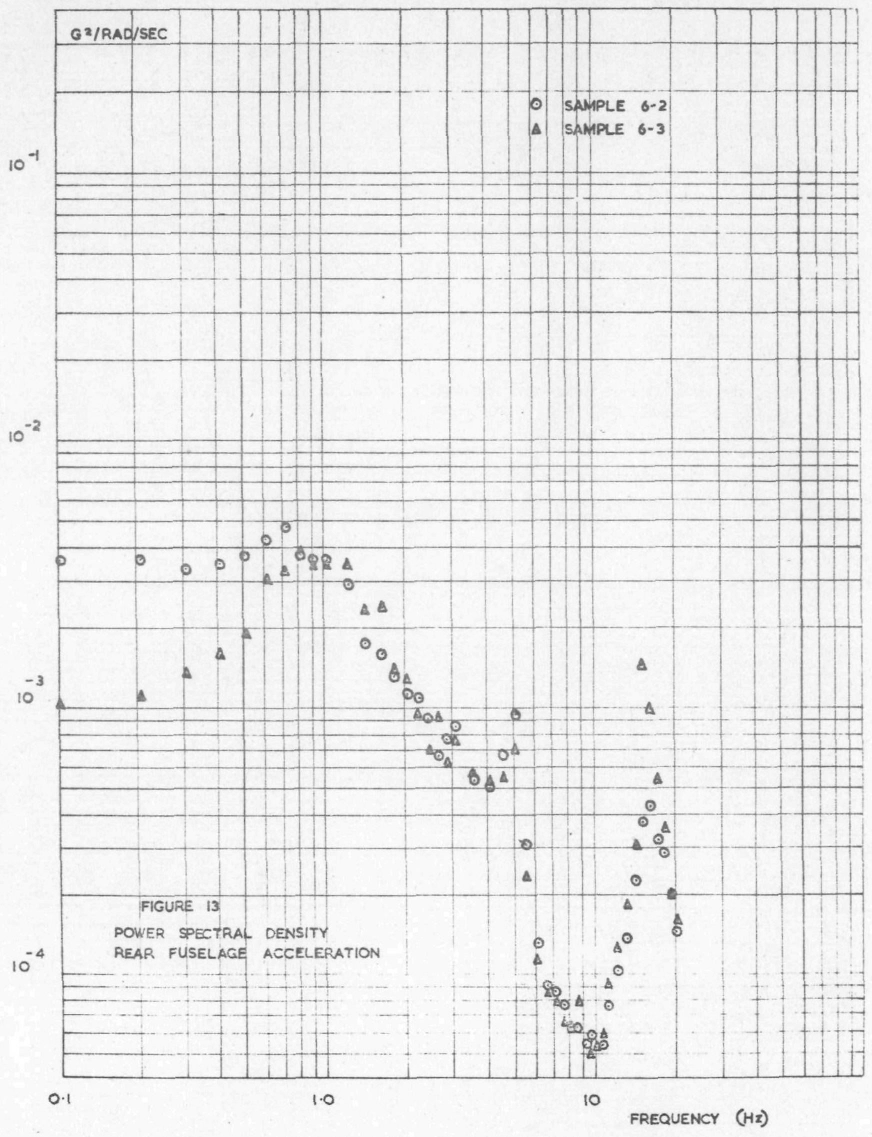

FIGURE 13 POWER SPECTRAL DENSITY REAR FUSELAGE ACCELERATION

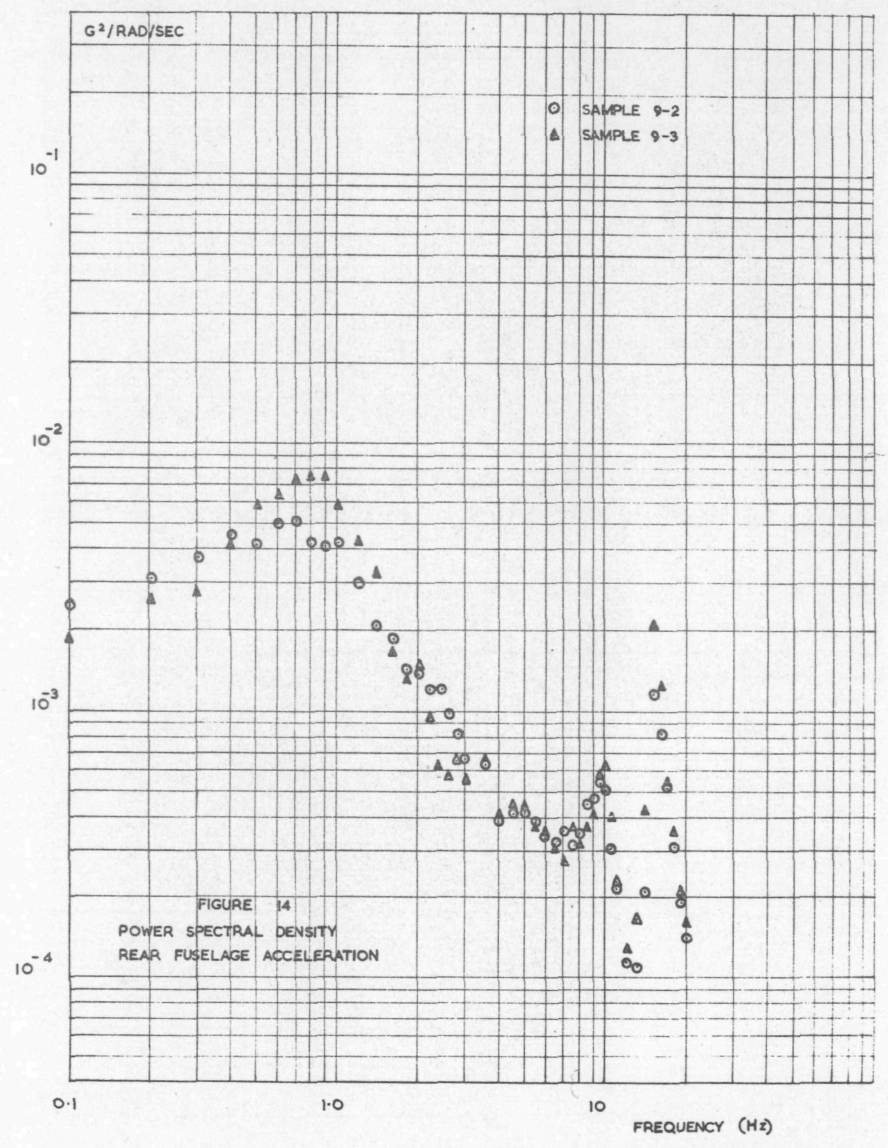

FIGURE 14 POWER SPECTRAL DENSITY REAR FUSELAGE ACCELERATION

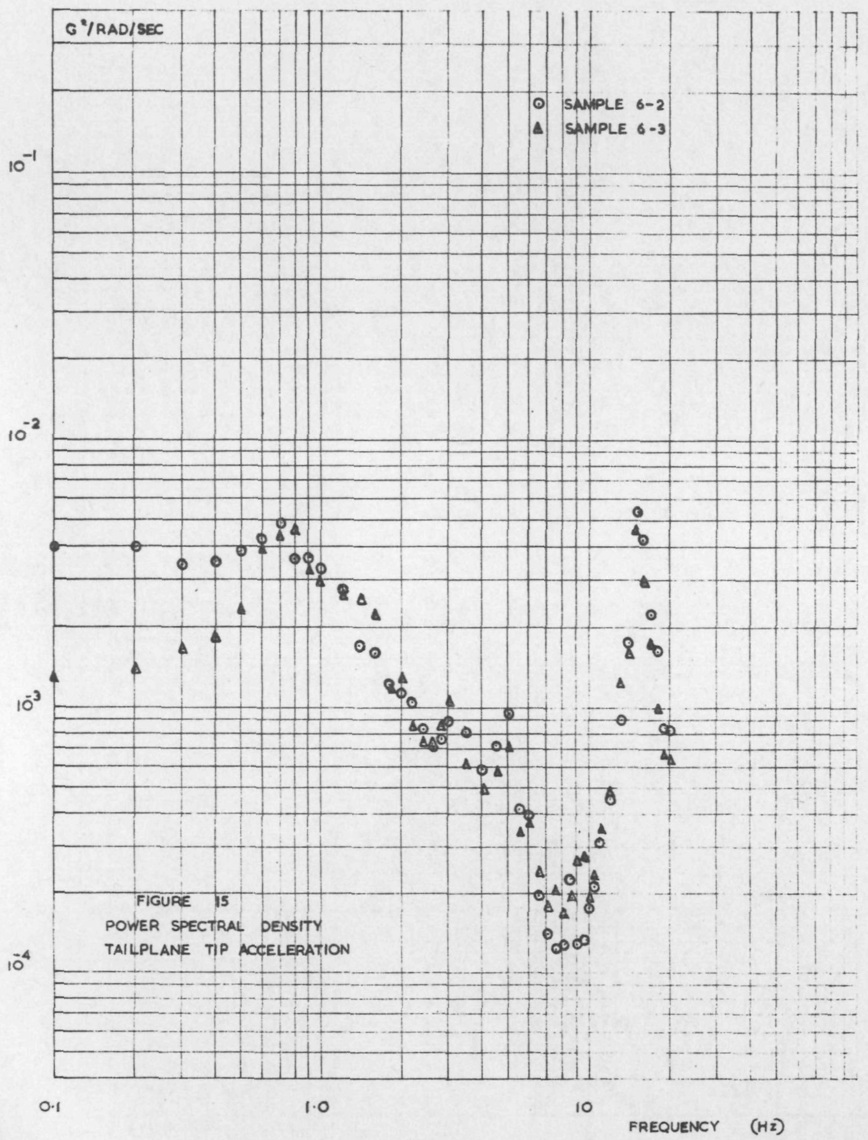

FIGURE 15 POWER SPECTRAL DENSITY TAILPLANE TIP ACCELERATION

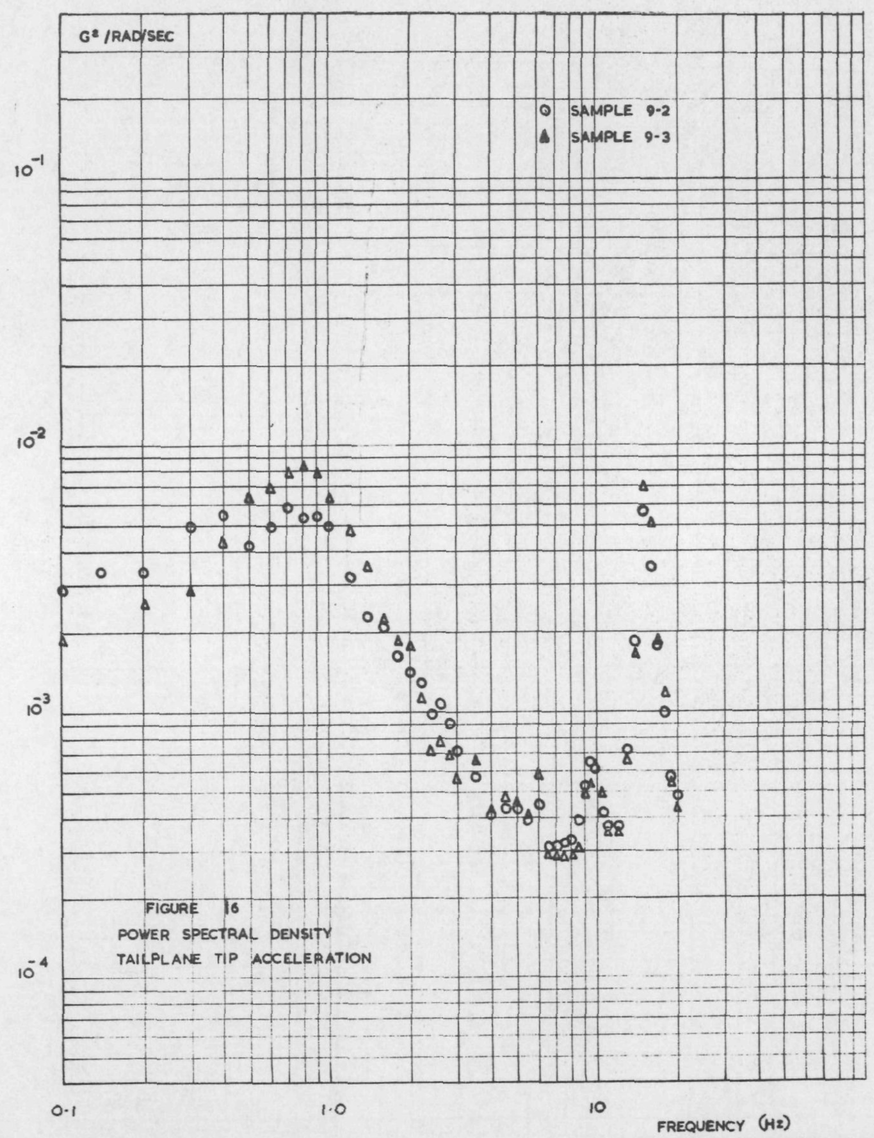

FIGURE 16 POWER SPECTRAL DENSITY TAILPLANE TIP ACCELERATION

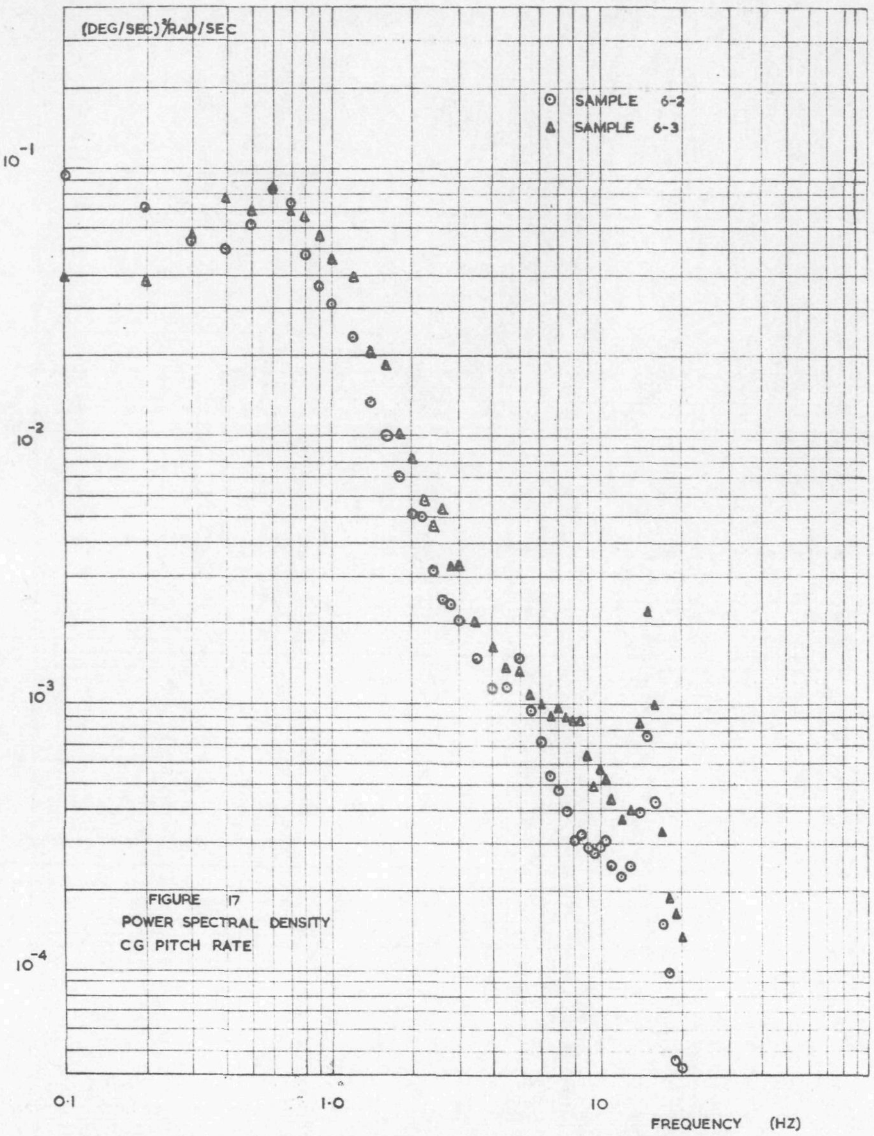

FIGURE 17 POWER SPECTRAL DENSITY CG PITCH RATE

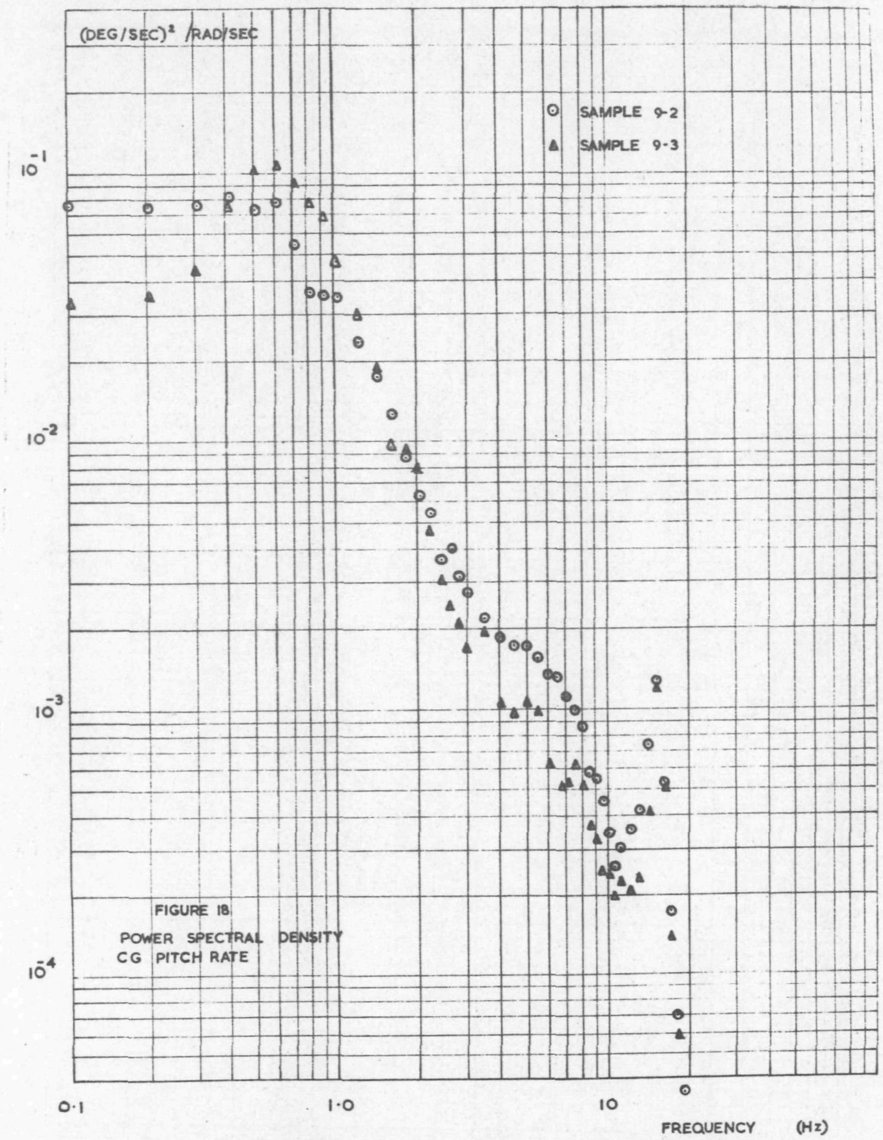

FIGURE 18 POWER SPECTRAL DENSITY CG PITCH RATE

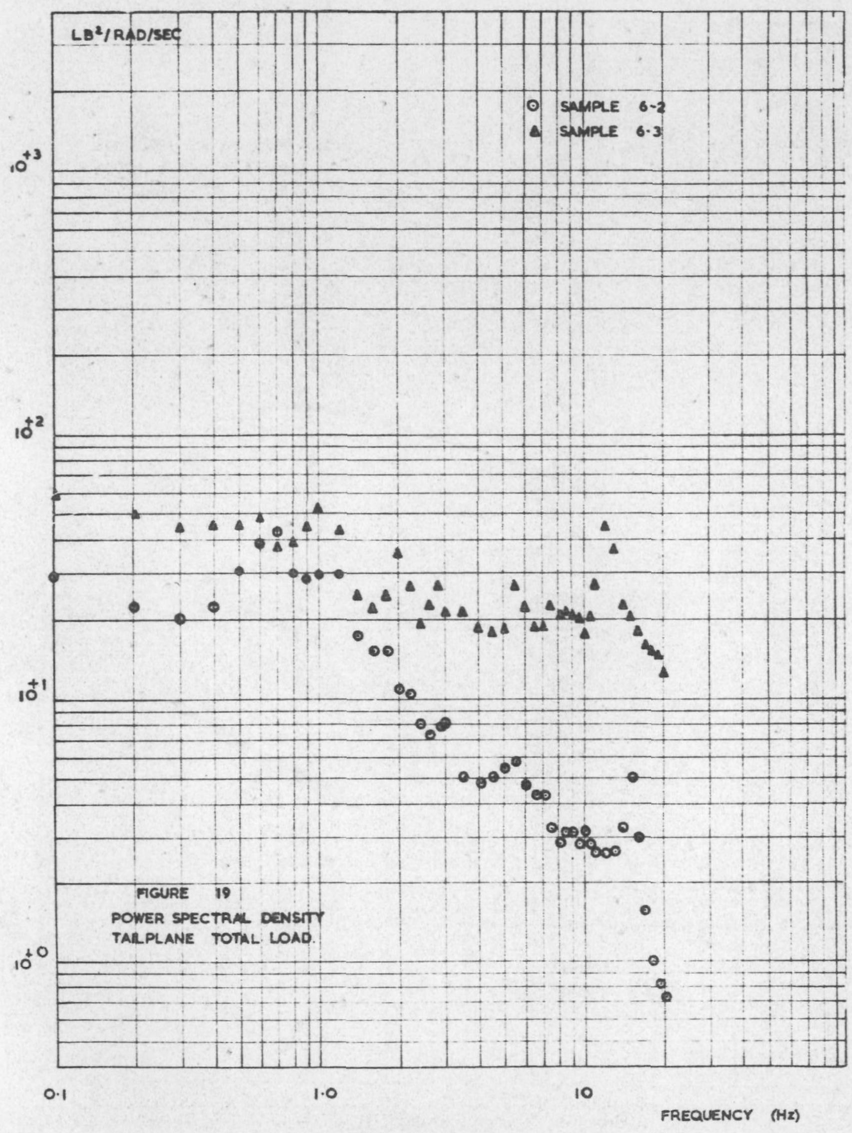

FIGURE 19 POWER SPECTRAL DENSITY TAILPLANE TOTAL LOAD

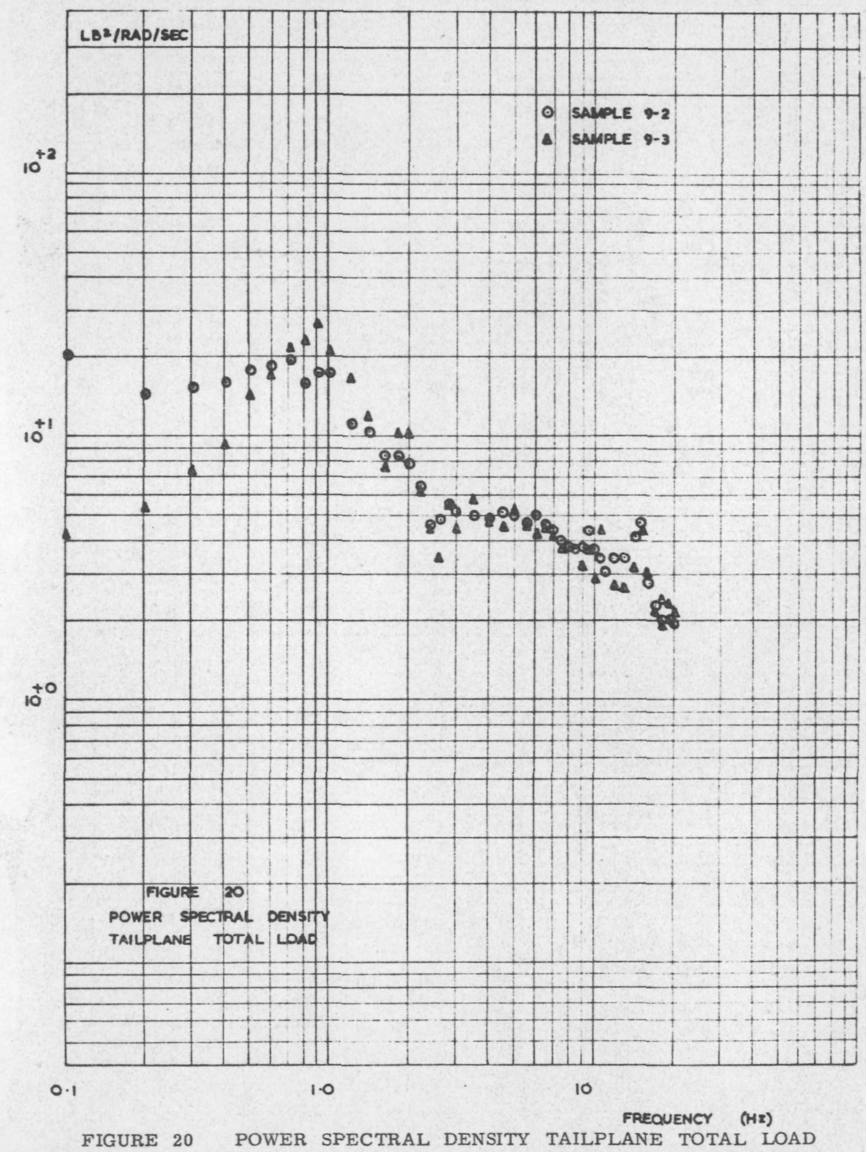

FIGURE 20 POWER SPECTRAL DENSITY TAILPLANE TOTAL LOAD

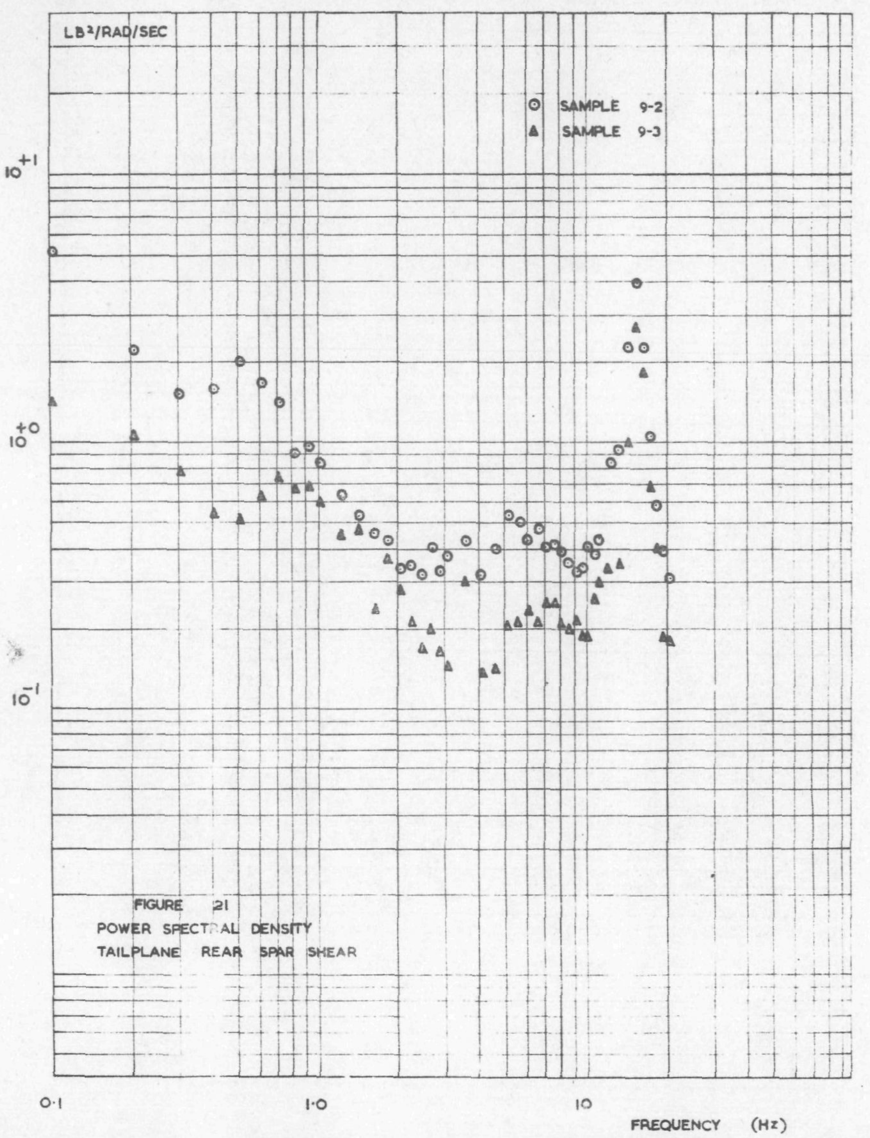

FIGURE 21 POWER SPECTRAL DENSITY TAILPLANE REAR SPAR SHEAR

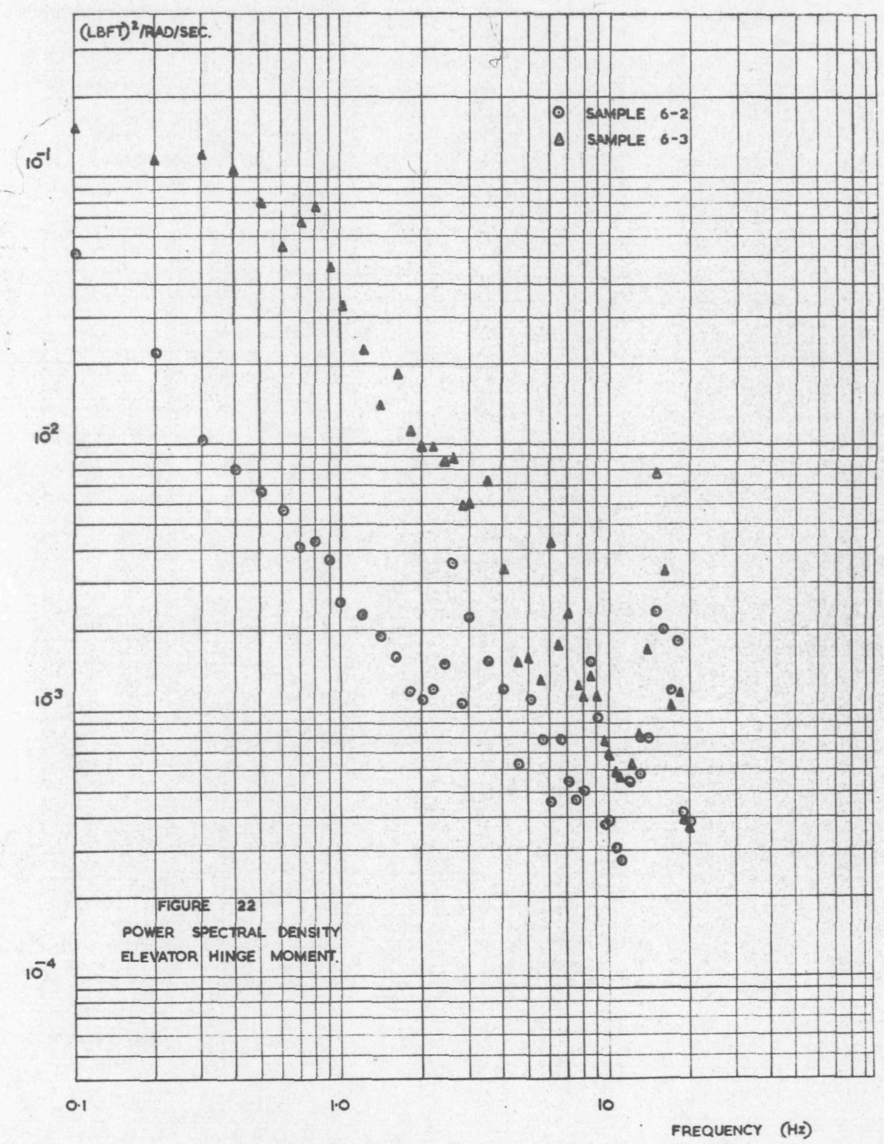

FIGURE 22 POWER SPECTRAL DENSITY ELEVATOR HINGE MOVEMENT

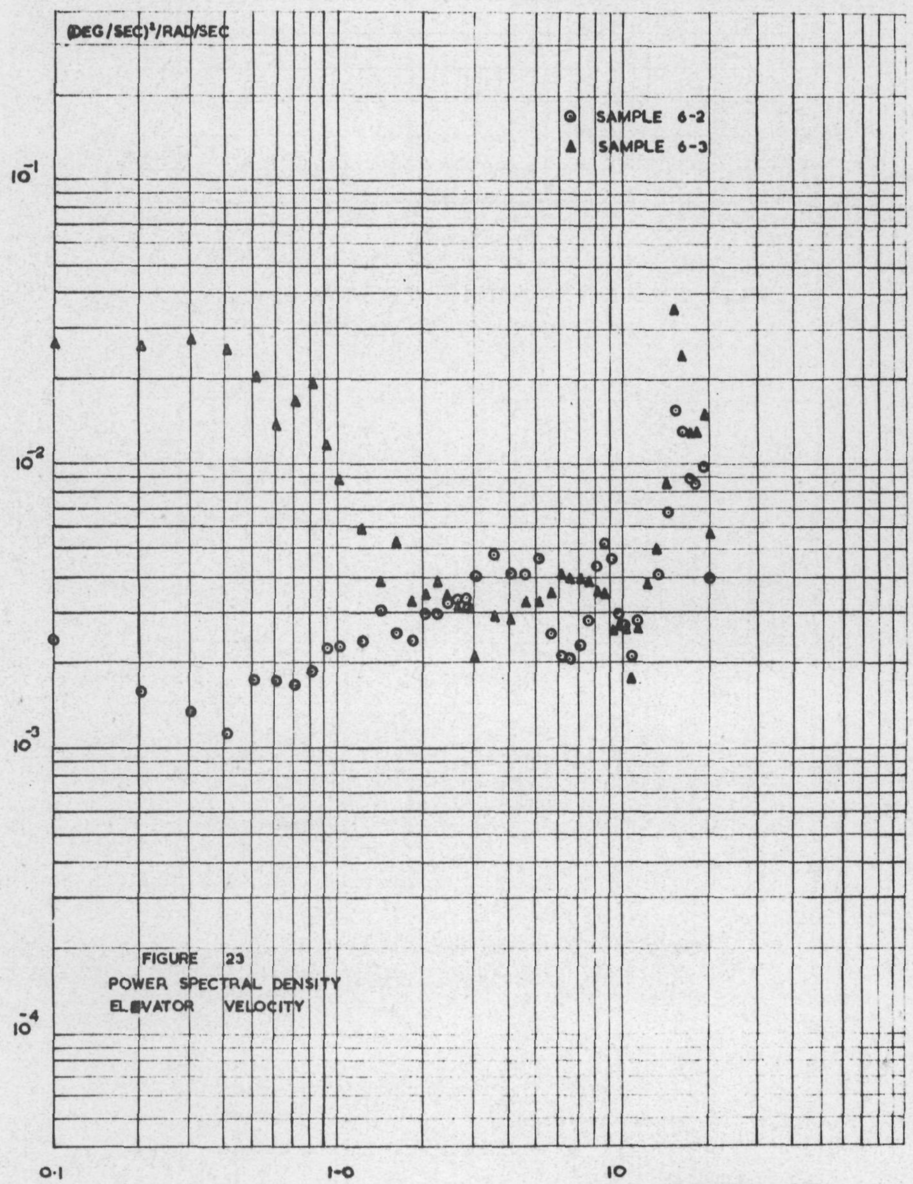

FIGURE 23 POWER SPECTRAL DENSITY ELEVATOR VELOCITY

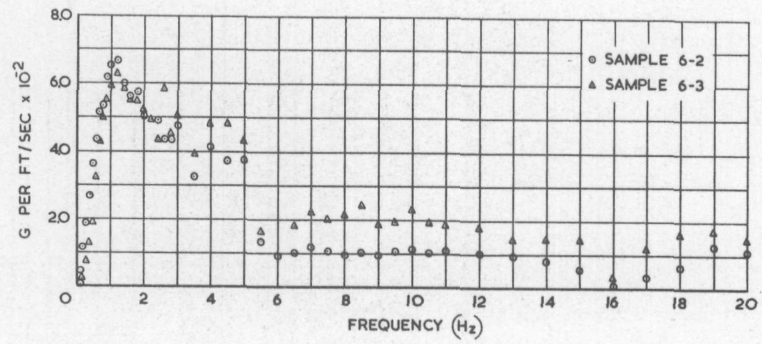

FIG.24. COHERENT AMPLITUDE SPECTRUM-C.G. ACCELERATION/GUST VELOCITY.

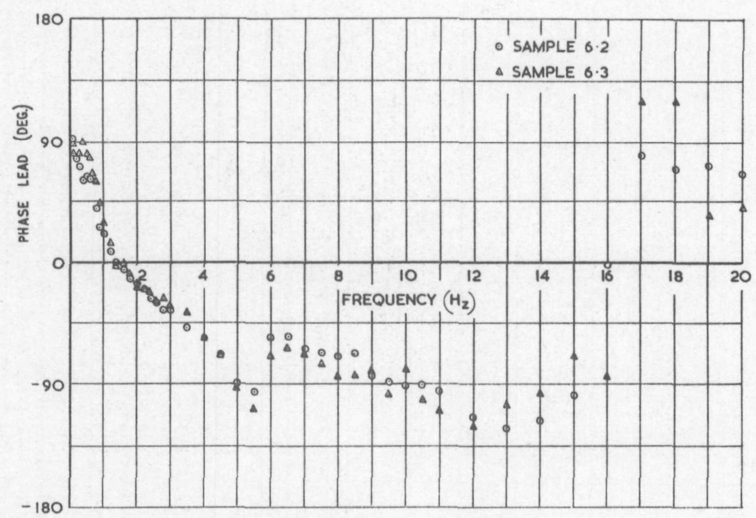

FIG.25. PHASE ANGLE SPECTRUM-C.G. ACCELERATION/GUST VELOCITY.

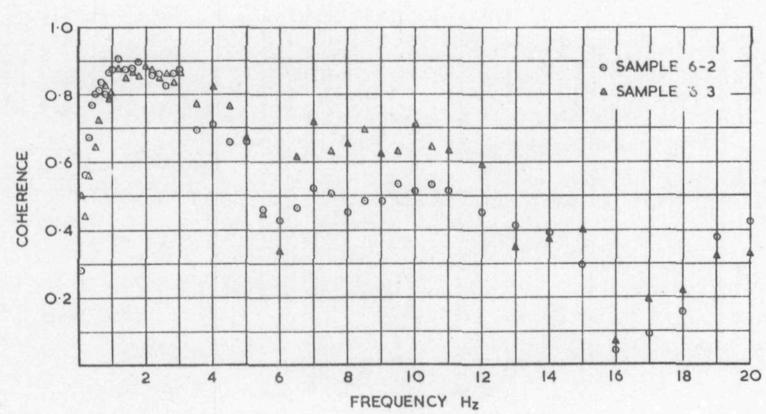

FIG.26. COHERENCE FUNCTION-C.G. ACCELERATION/GUST VELOCITY.

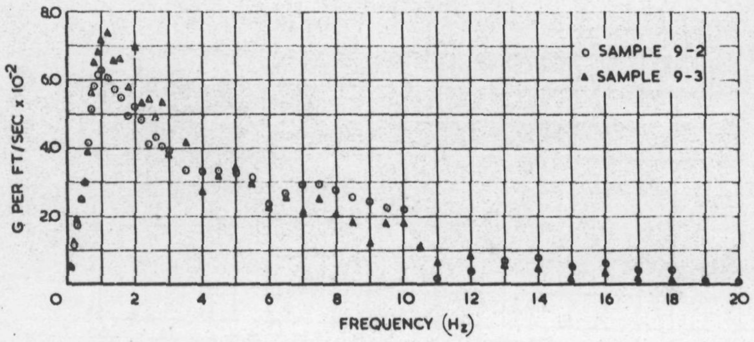

FIG.27. COHERENT AMPLITUDE SPECTRUM-C.G. ACCELERATION/GUST VELOCITY.

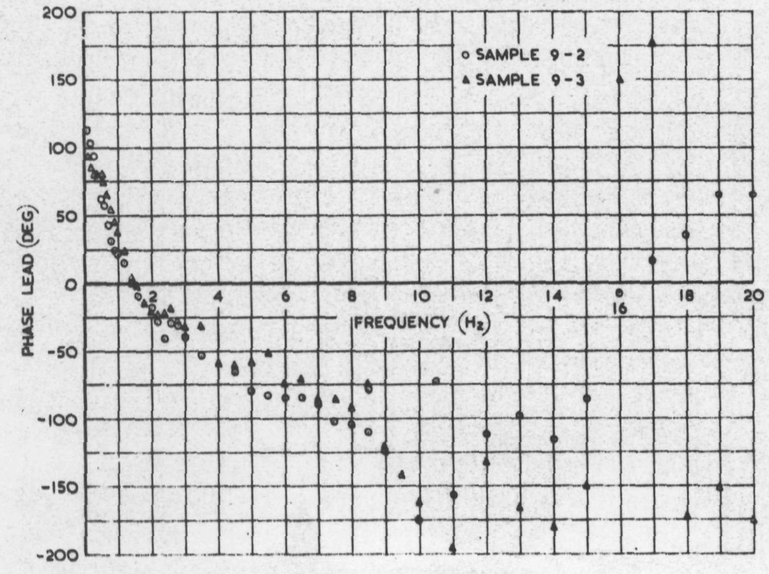

FIG.28. PHASE ANGLE SPECTRUM-C.G. ACCELERATION/GUST VELOCITY.

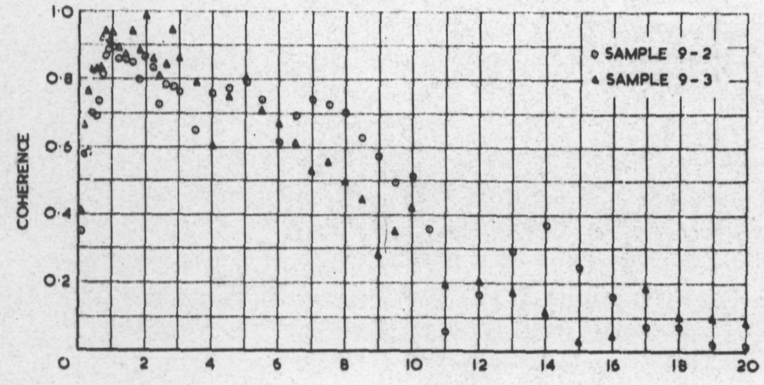

FIG.29. COHERENCE FUNCTION-C.G. ACCELERATION/GUST VELOCITY.

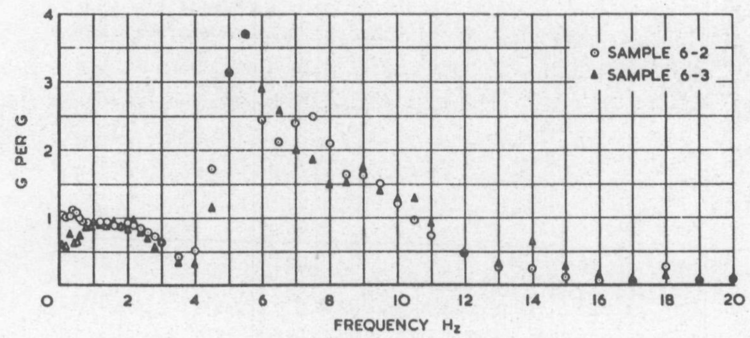

FIG.30. COHERENT AMPLITUDE SPECTRUM-WINGTIP ACCELERATION/C.G. ACCELERATION.

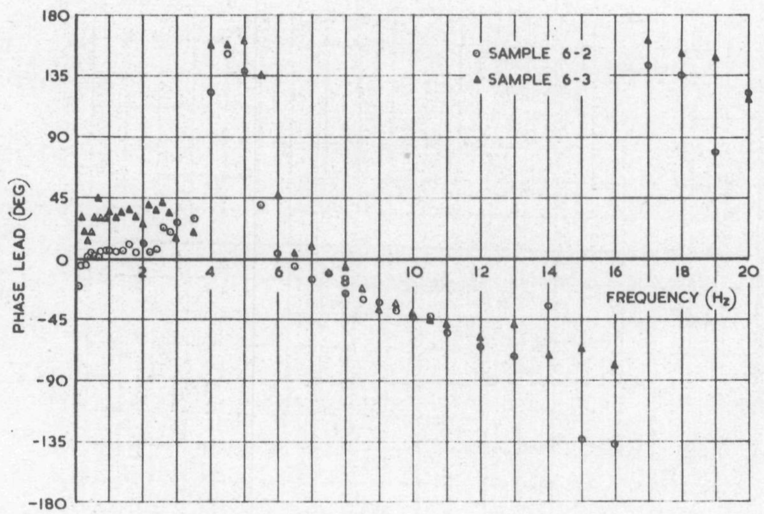

FIG.31. PHASE ANGLE SPECTRUM-WINGTIP ACCELERATION/C.G. ACCELERATION.

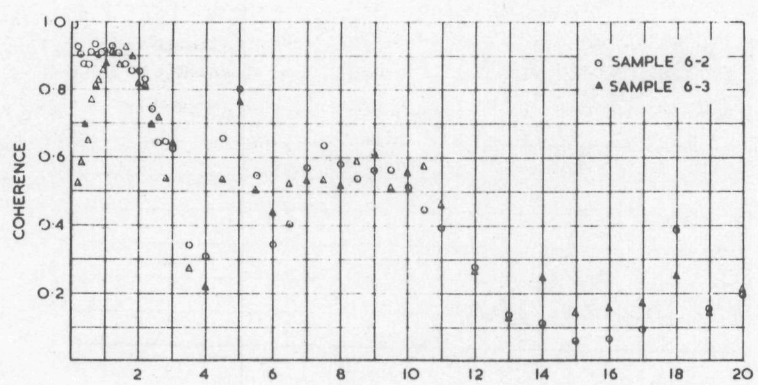

FIG.32. COHERENCE FUNCTION-WINGTIP ACCELERATION/ C.G. ACCELERATION

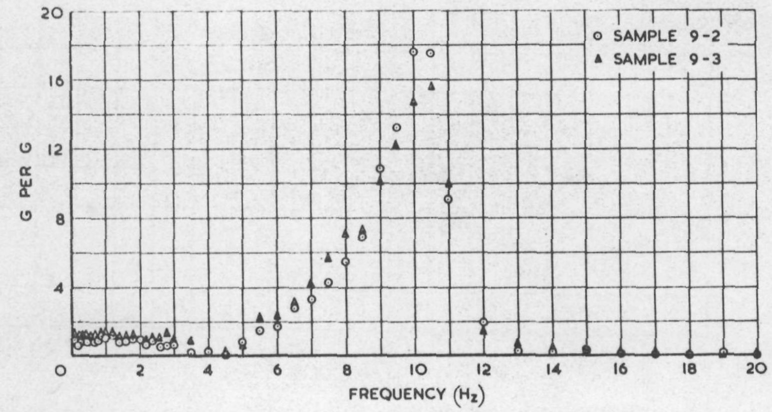

FIG.33. COHERENT AMPLITUDE SPECTRUM-WINGTIP ACCELERATION/C.G. ACCELERATION.

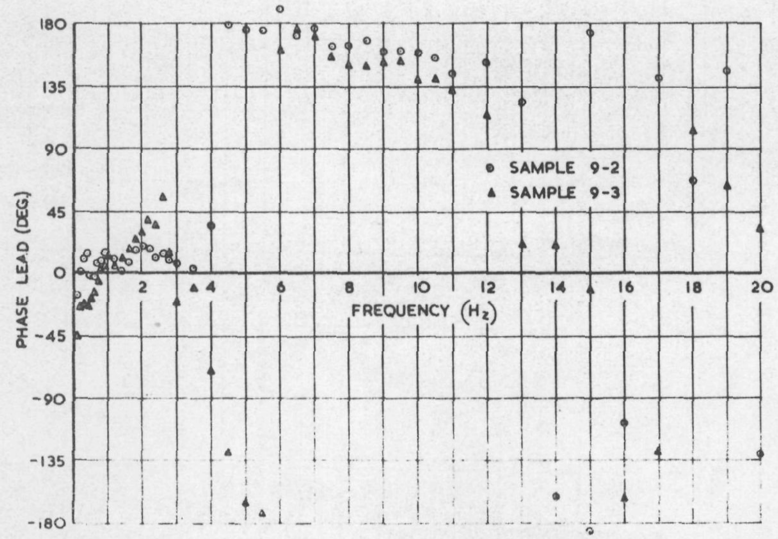

FIG.34. PHASE ANGLE SPECTRUM-WINGTIP ACCELERATION/C.G. ACCELERATION.

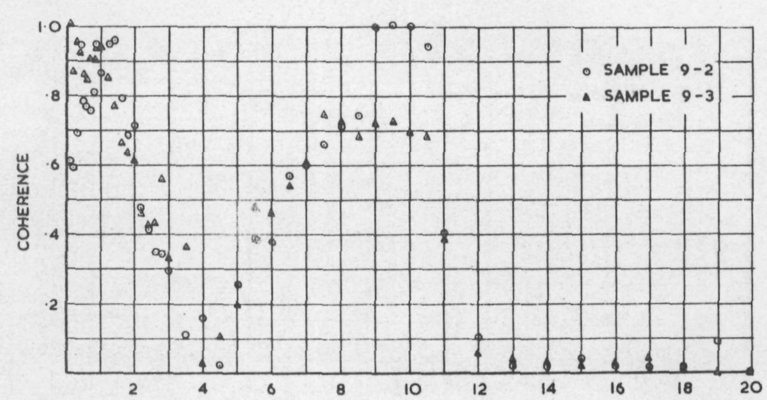

FIG.35. COHERENCE FUNCTION-WINGTIP ACCELERATION/ C.G. ACCELERATION

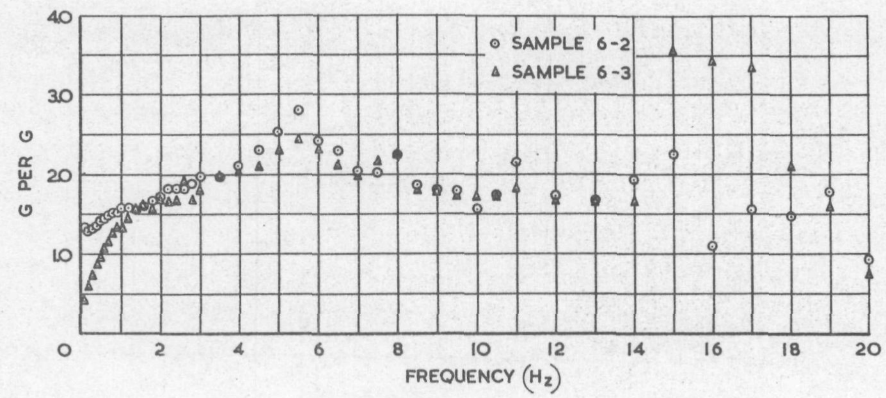

FIG.36. COHERENT AMPLITUDE SPECTRUM-REAR FUSELAGE

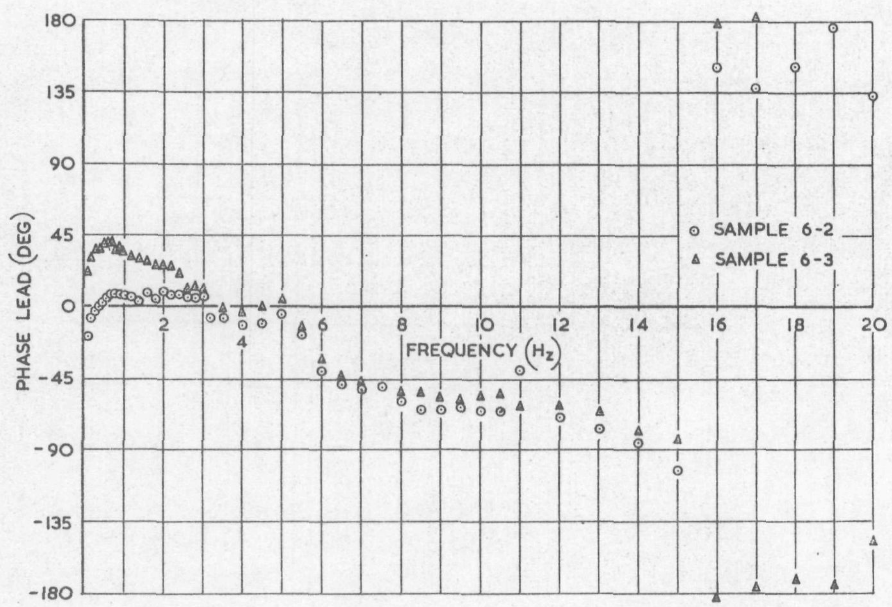

FIG.37. PHASE ANGLE SPECTRUM-REAR FUSE.
ACCELERATION/C.G ACCELERATION.

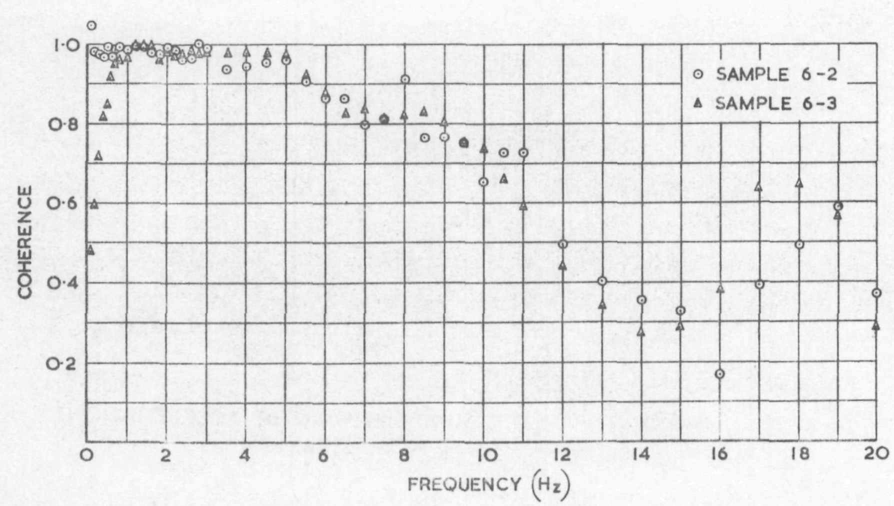

FIG.38. COHERENCE FUNCTION-REAR FUSE.
ACCELERATION/C.G. ACCELERATION.

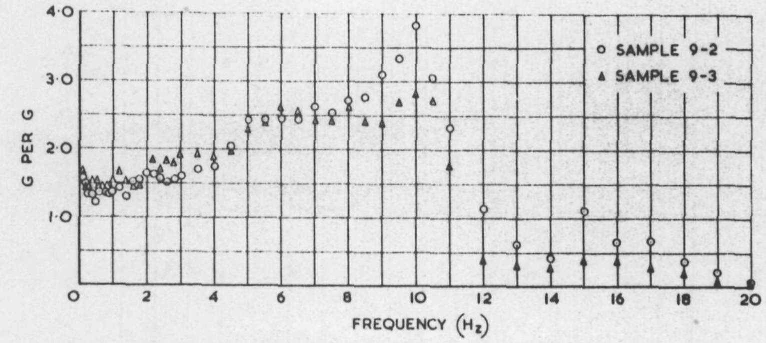

FIG.39. COHERENT AMPLITUDE SPECTRUM-REAR FUSELAGE ACCELERATION/C.G ACCELERATION.

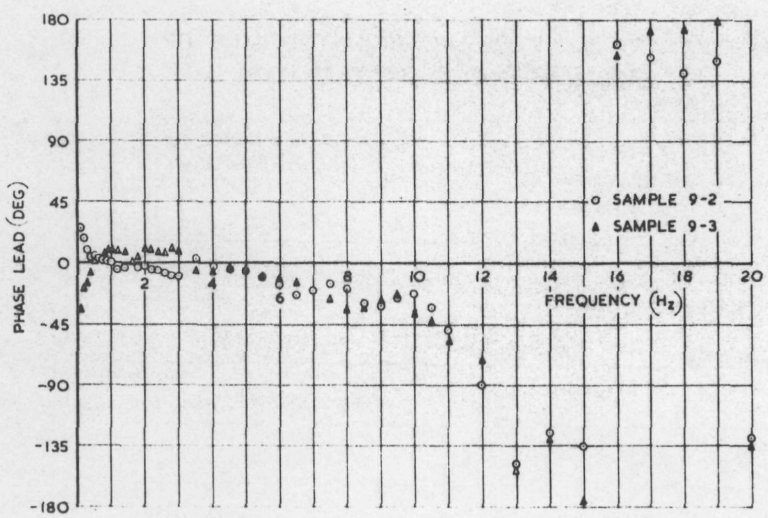

FIG.40. PHASE ANGLE SPECTRUM-REAR FUSE ACCELERATION/C.G ACCELERATION.

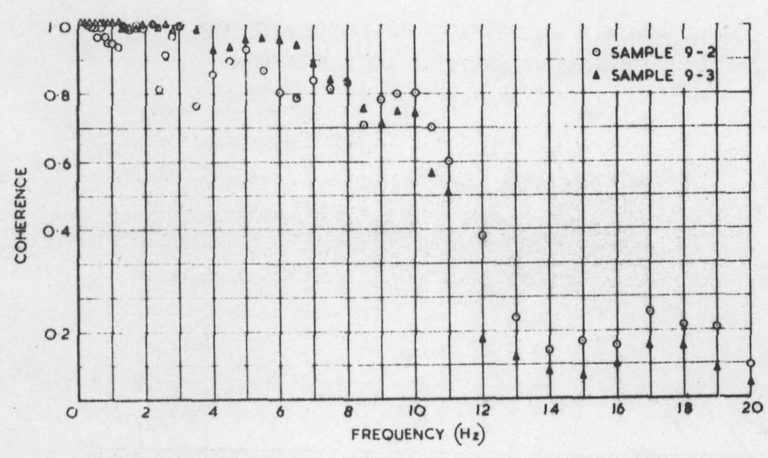

FIG.41. COHERENCE FUNCTION-REAR FUSELAGE ACCELERATION/C.G. ACCELERATION.

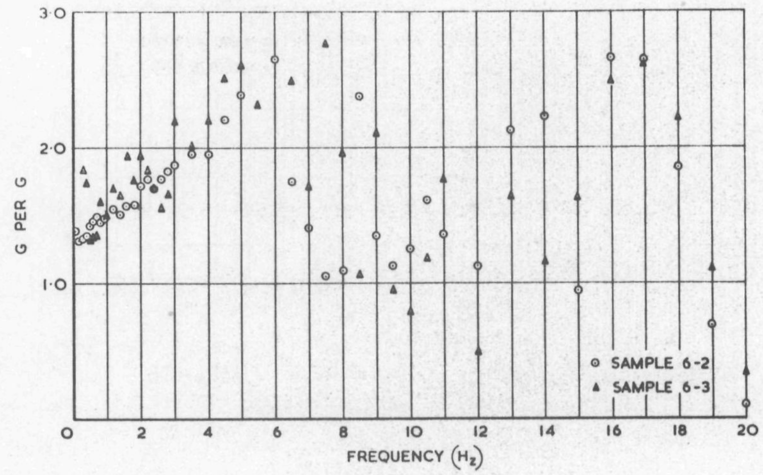

FIG.42. COHERENT AMPLITUDE SPECTRUM-TAILPLANE TIP ACCELERATION/C.G. ACCELERATION.

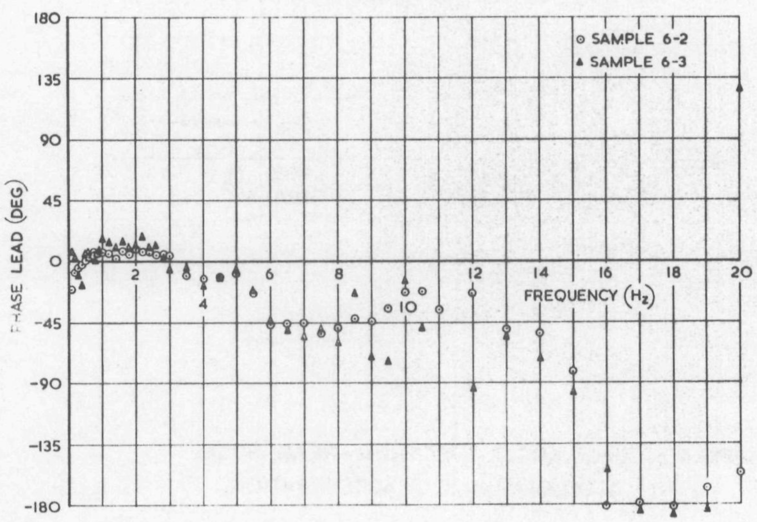

FIG.43. PHASE ANGLE SPECTRUM-TAILPLANE TIP ACCELERATION/C.G. ACCELERATION.

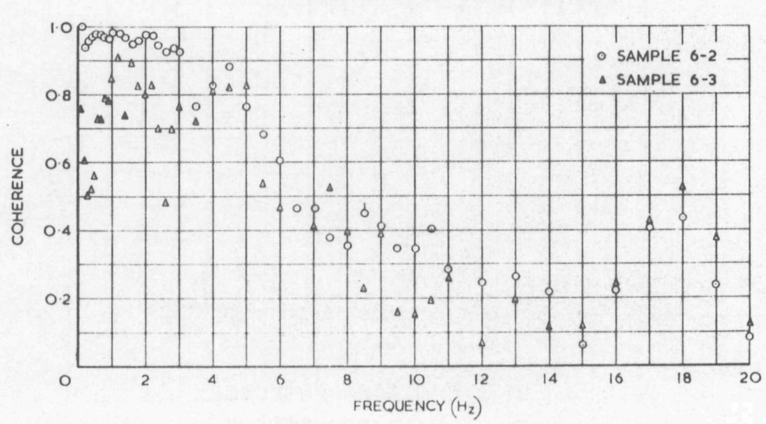

FIG.44. COHERENCE FUNCTION-TAILPLANE TIP ACCELERATION/C.G. ACCELERATION.

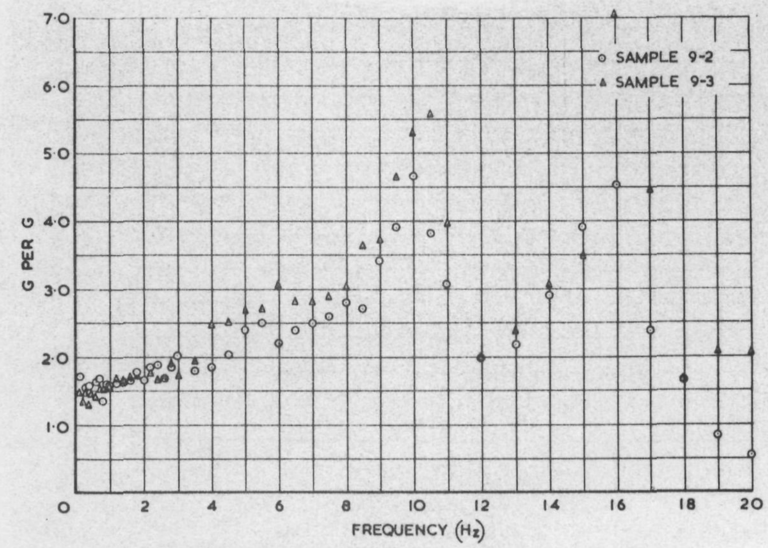

FIG.45. COHERENT AMPLITUDE SPECTRUM-TAILPLANE TIP ACCELERATION/C.G ACCELERATION.

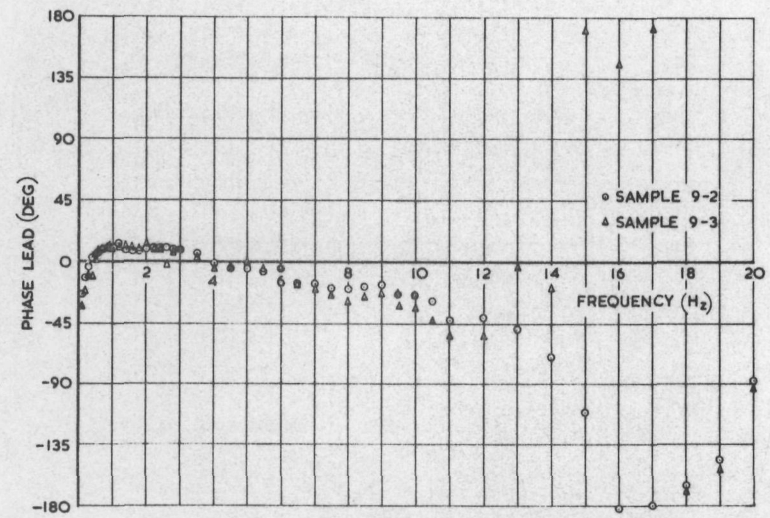

FIG.46. PHASE ANGLE SPECTRUM-TAILPLANE TIP ACCELERATION/C.G. ACCELERATION.

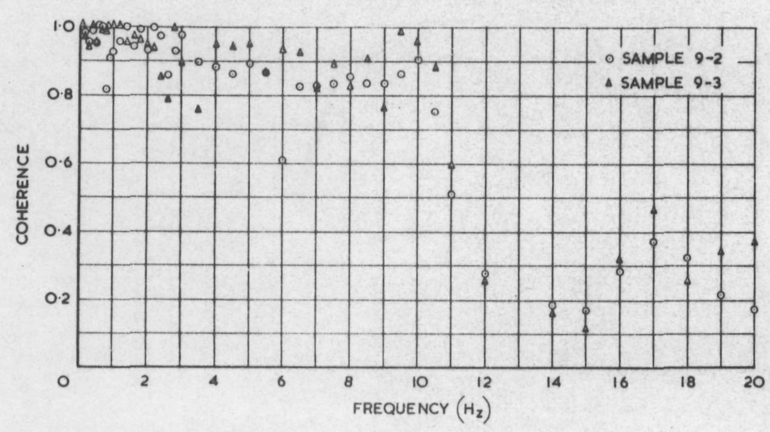

FIG.47. COHERENCE FUNCTION-TAILPLANE TIP ACCELERATION/C.G ACCELERATION.

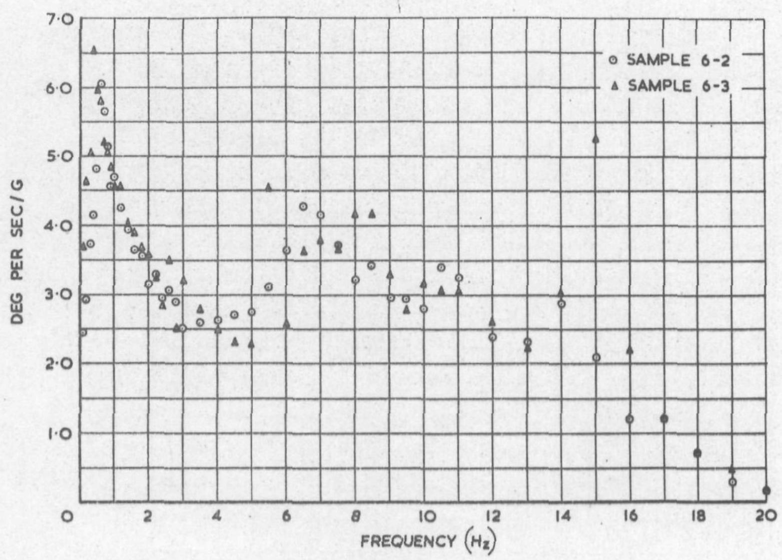

FIG.48. COHERENT AMPLITUDE SPECTRUM-
PITCH RATE/C.G. ACCELERATION.

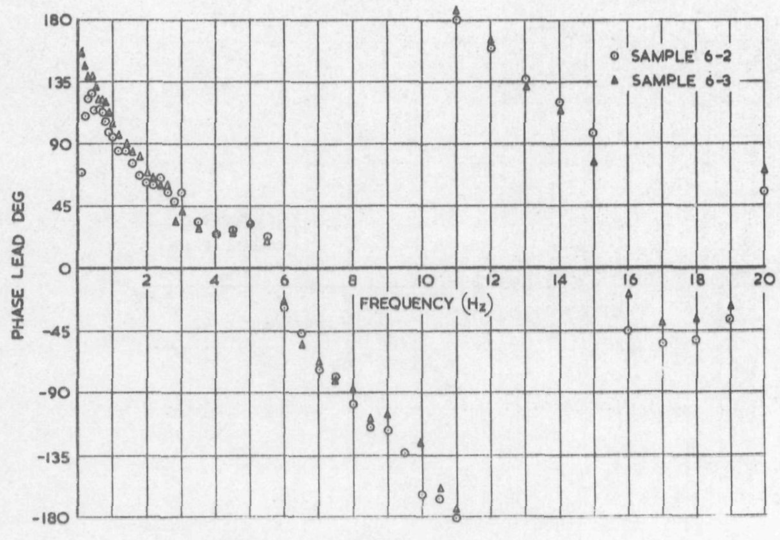

FIG.49. PHASE ANGLE SPECTRUM-
C.G. PITCH RATE/C.G. ACCELERATION.

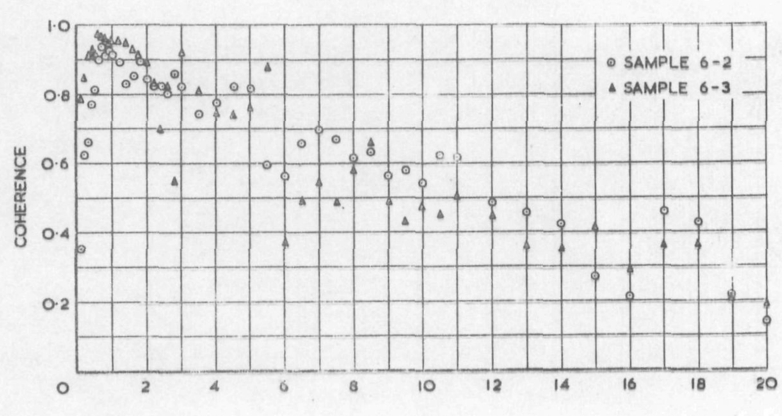

FIG.50. COHERENCE FUNCTION-
C.G. PITCH RATE/C.G. ACCELERATION.

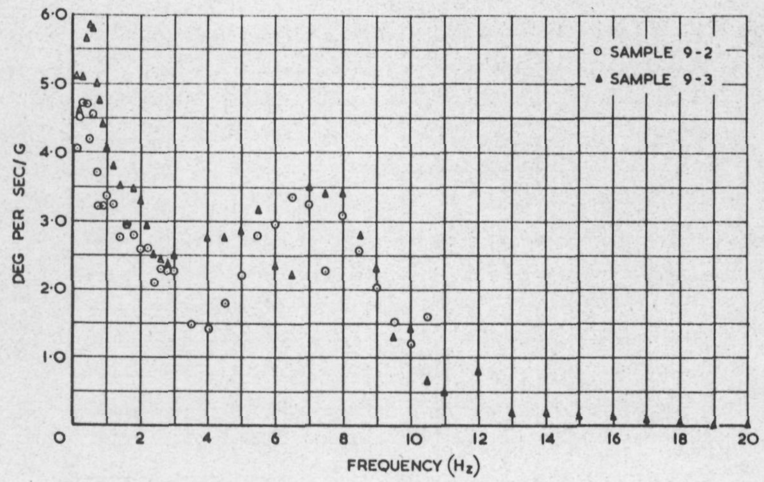

FIG. 51. COHERENT AMPLITUDE SPECTRUM – C.G. PITCH RATE/C.G. ACCELERATION.

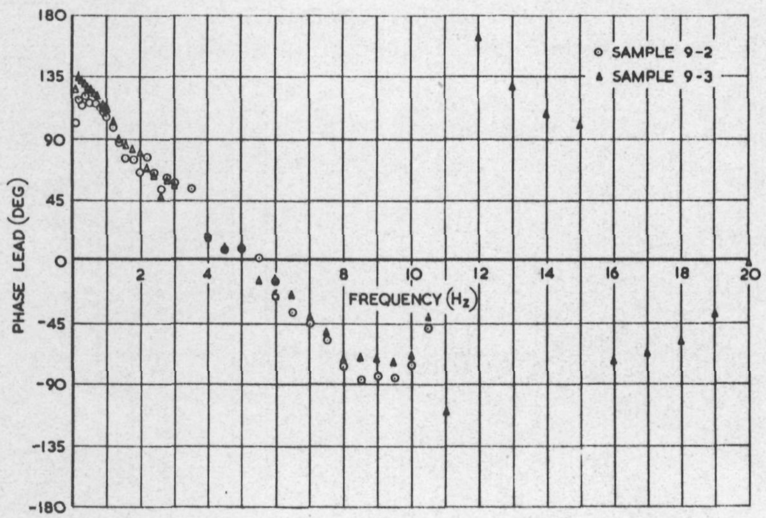

FIG. 52. PHASE ANGLE SPECTRUM – C.G. PITCH RATE/C.G ACCELERATION.

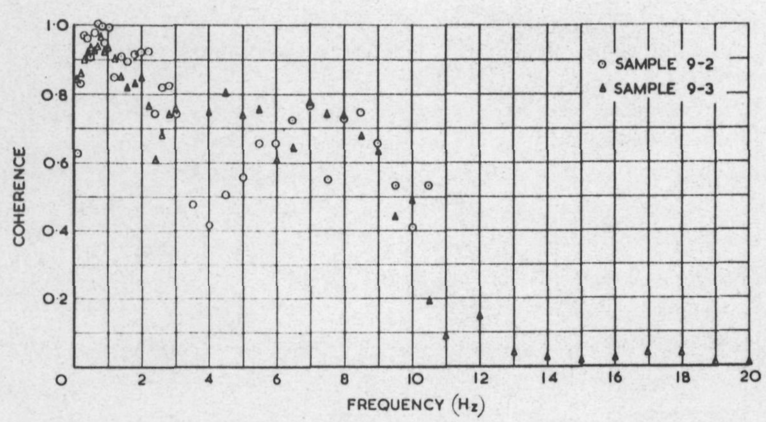

FIG. 53. COHERENCE FUNCTION – C.G. PITCH RATE/C.G. ACCELERATION.

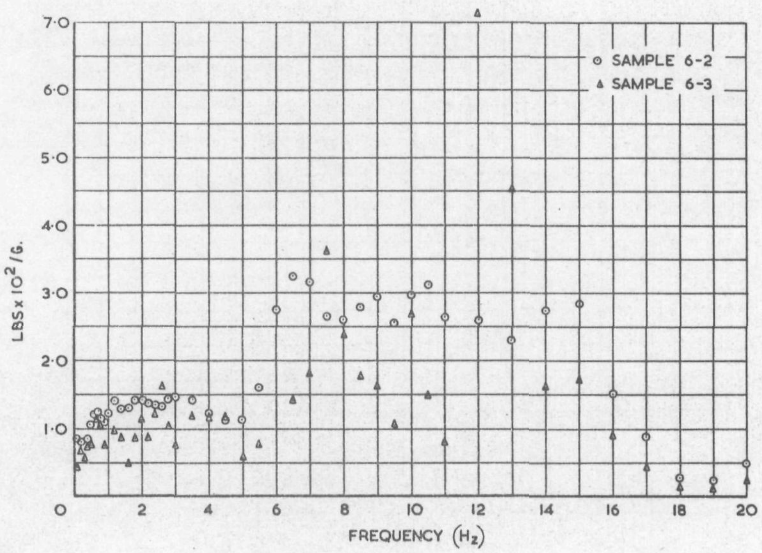

FIG.54. COHERENT AMPLITUDE SPECTRUM - TAILPLANE TOTAL LOAD/C.G. ACCELERATION.

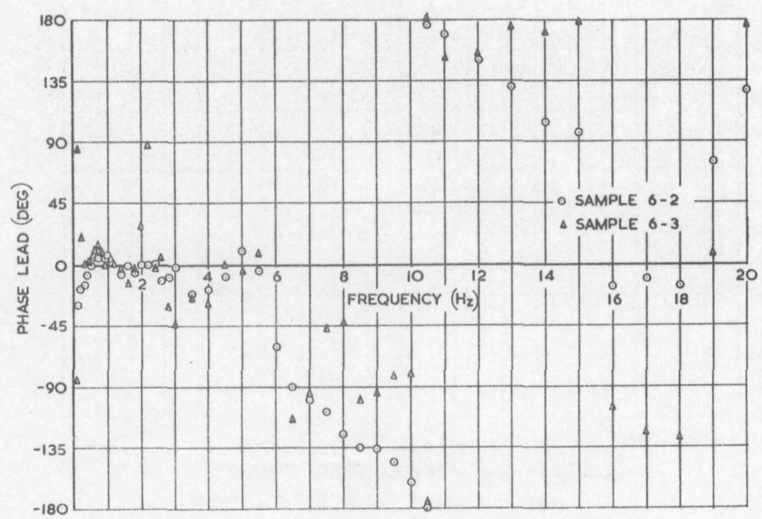

FIG.55. PHASE ANGLE SPECTRUM - TAILPLANE TOTAL LOAD/C.G. ACCELERATION.

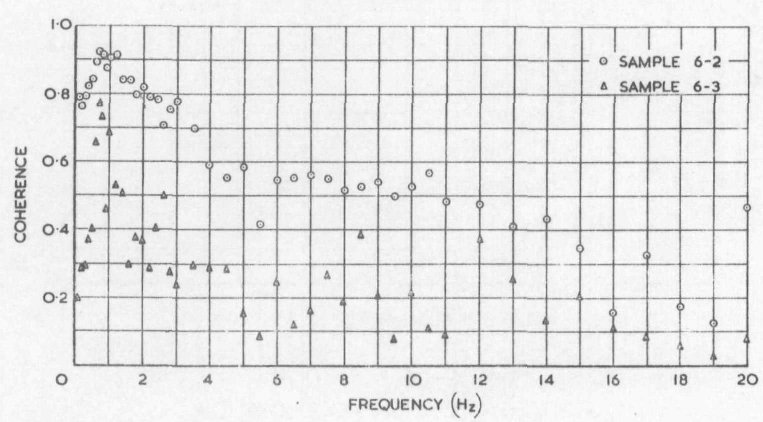

FIG.56. COHERENCE FUNCTION TAILPLANE - TOTAL LOAD/C.G. ACCELERATION.

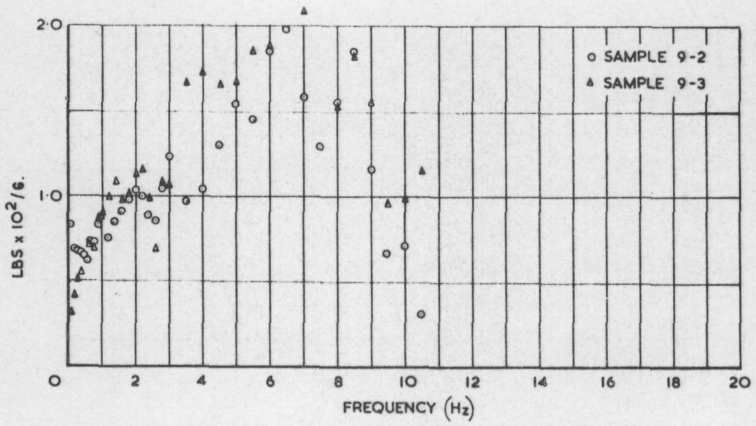

FIG.57. COHERENT AMPLITUDE SPECTRUM - TAILPLANE TOTAL LOAD/C.G. ACCELERATION.

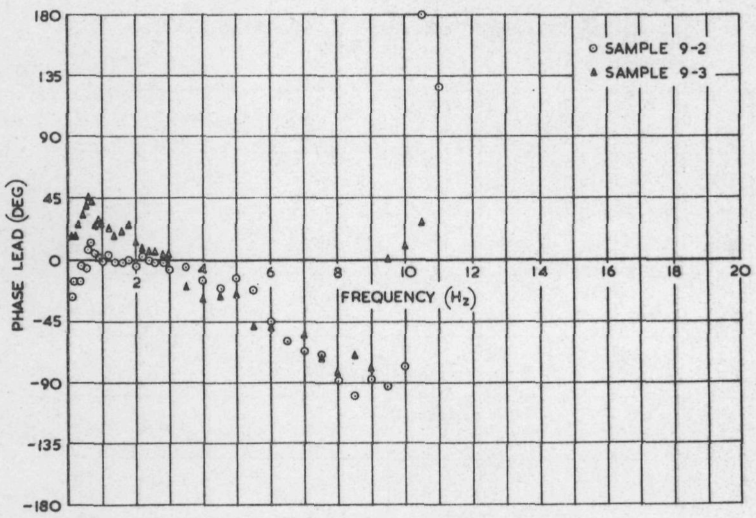

FIG.58. PHASE ANGLE SPECTRUM - TAILPLANE TOTAL LOAD/C.G. ACCELERATION.

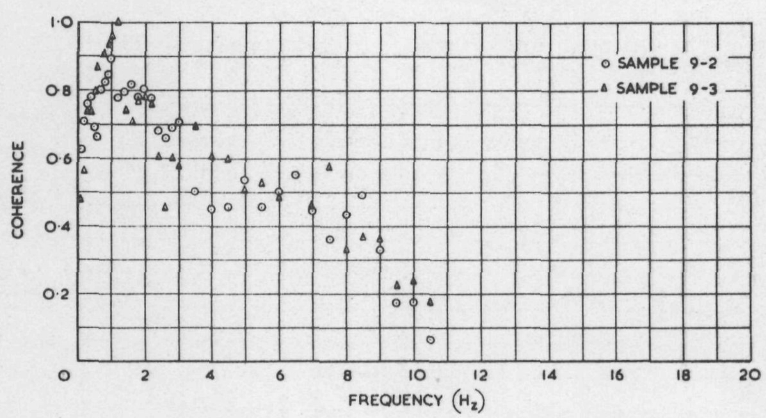

FIG.59. COHERENCE FUNCTION TAILPLANE - TOTAL LOAD/C.G. ACCELERATION.

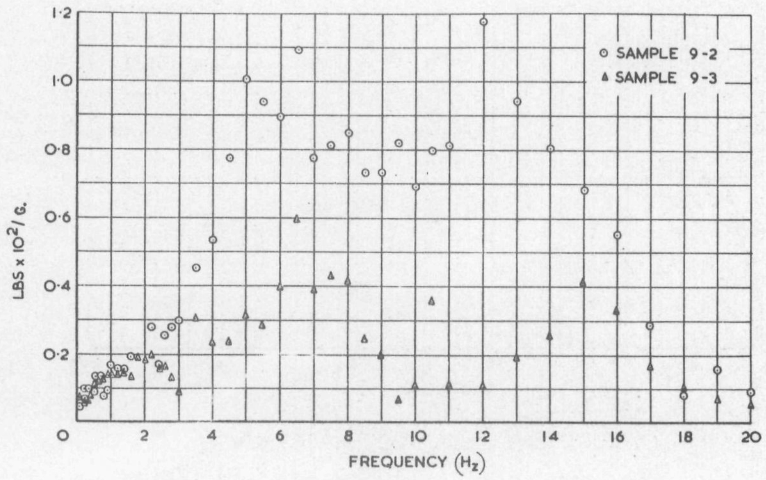

FIG.60. COHERENT AMPLITUDE SPECTRUM -
T/P REAR SPAR SHEAR/C.G. ACCELERATION.

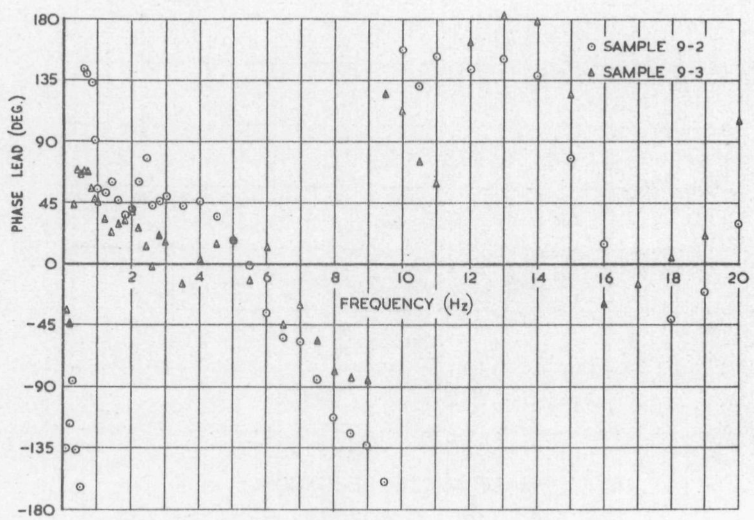

FIG.61. PHASE ANGLE SPECTRUM -
T/P REAR SPAR SHEAR/C.G. ACCELERATION.

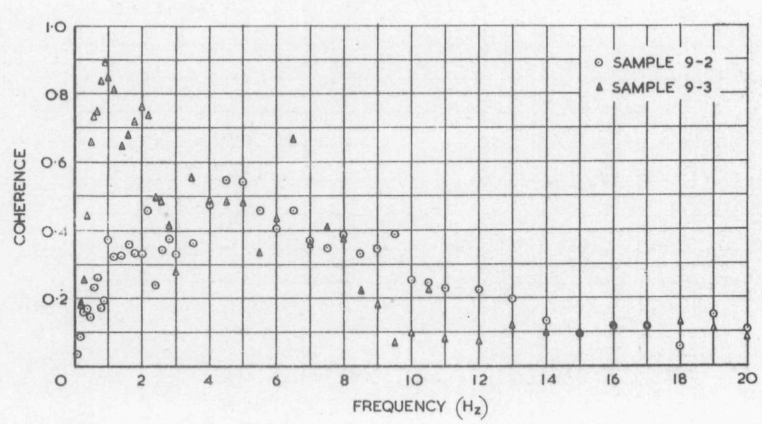

FIG.62. COHERENCE FUNCTION-TAILPLANE
REAR SPAR SHEAR/C.G. ACCELERATION.

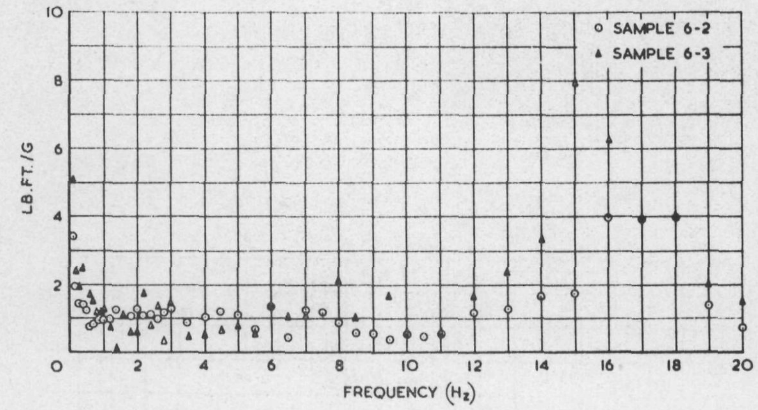

FIG.63. COHERENT AMPLITUDE SPECTRUM-
ELEVATOR H.M/C.G. ACCELERATION.

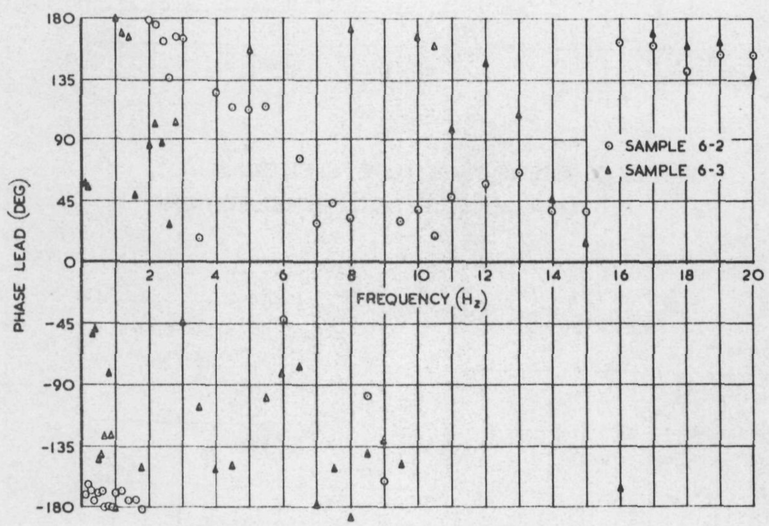

FIG.64. PHASE ANGLE SPECTRUM-
ELEVATOR HINGE MOMENT.

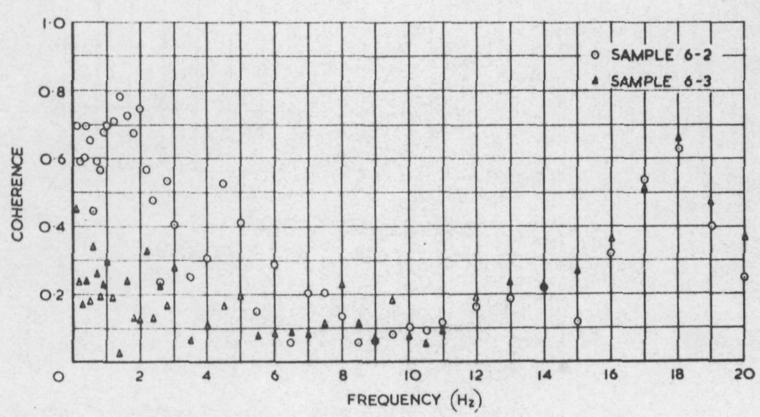

FIG.65. COHERENCE FUNCTION-ELEVATOR HINGE MOMENT.

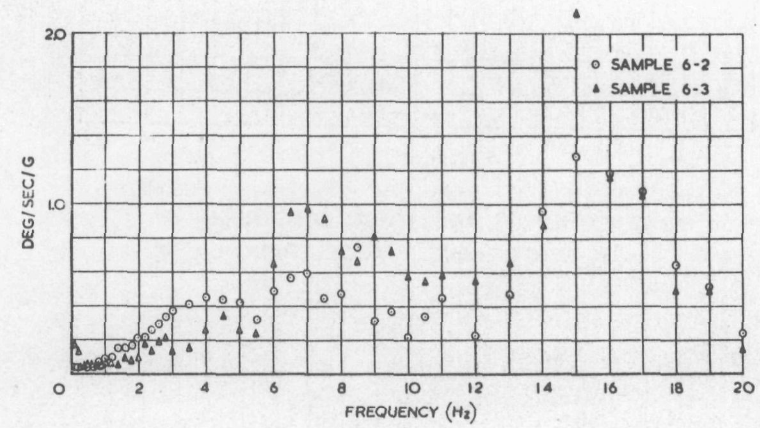

FIG.66. COHERENT AMPLITUDE SPECTRUM–
ELEVATOR VELOCITY/C.G. ACCELERATION.

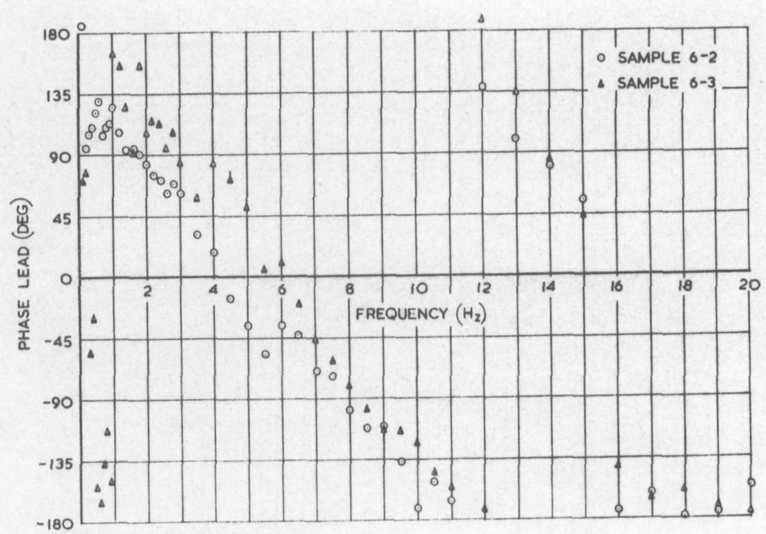

FIG.67. PHASE ANGLE SPECTRUM–
ELEVATOR VELOCITY/C.G. ACCELERATION.

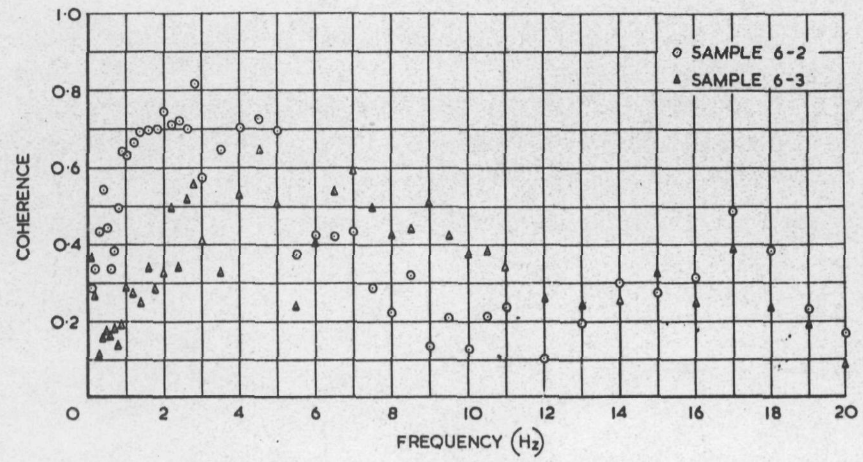

FIG.68. COHERENCE FUNCTION - ELEVATOR VELOCITY/C.G. ACCELERATION.

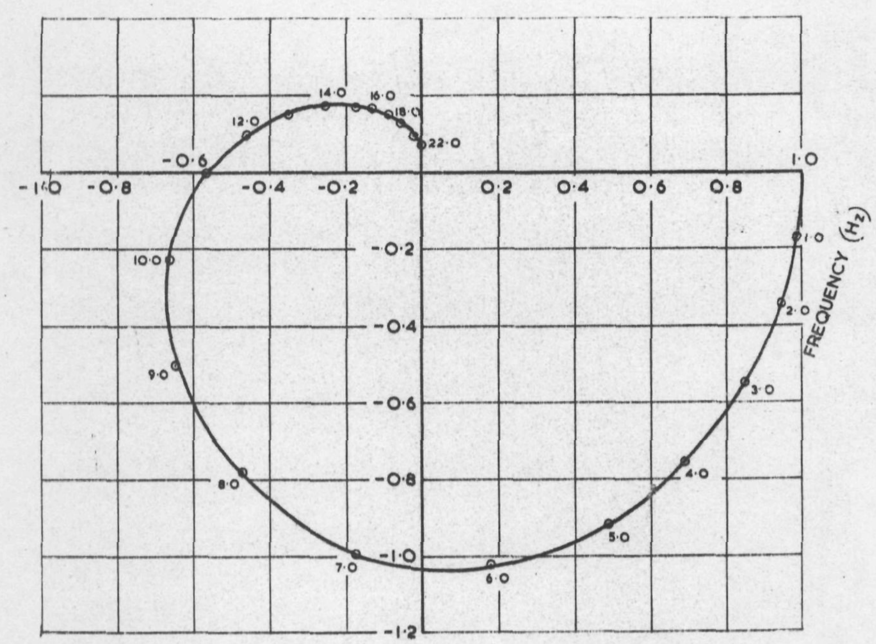

FIG.69. TRANSFER FUNCTION OF C.G. ACCELEROMETER FROM GROUND CALIBRATION (CORRECTED OUTPUT PER G INPUT.)